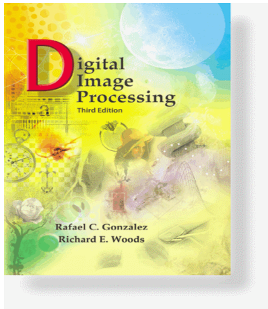

Chapter 4
Filtering in the Frequency Domain

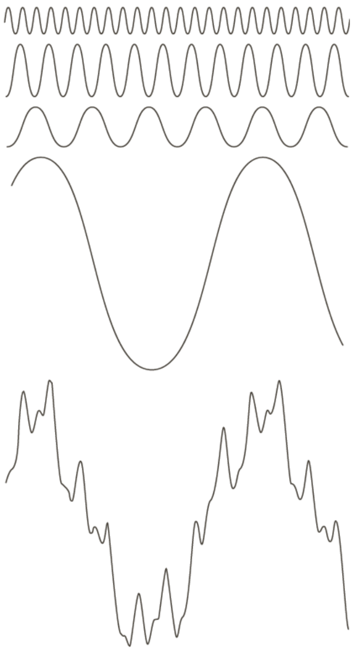

FIGURE 4.1 The function at the bottom is the sum of the four functions above it. Fourier's idea in 1807 that periodic functions could be represented as a weighted sum of sines and cosines was met with skepticism.

© 1992–2008 R. C. Gonzalez & R. E. Woods

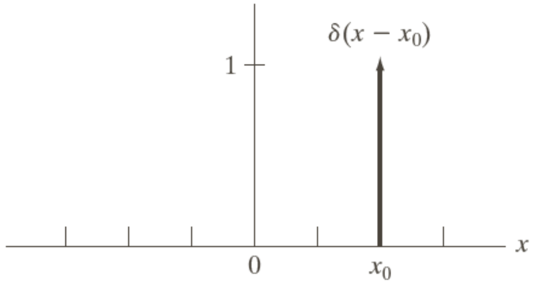

FIGURE 4.2 A unit discrete impulse located at $x = x_0$. Variable x is discrete, and δ is 0 everywhere except at $x = x_0$.

© 1992–2008 R. C. Gonzalez & R. E. Woods

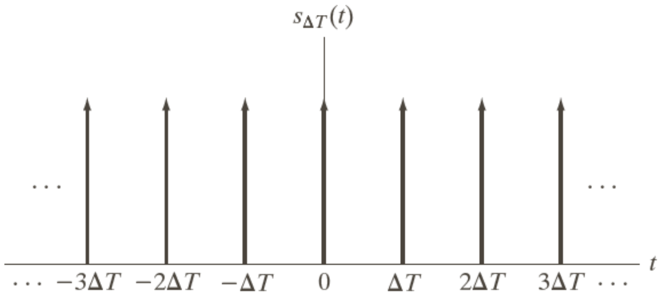

FIGURE 4.3 An impulse train.

© 1992–2008 R. C. Gonzalez & R. E. Woods

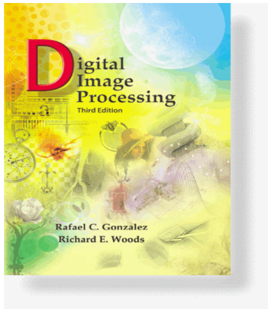

Chapter 4
Filtering in the Frequency Domain

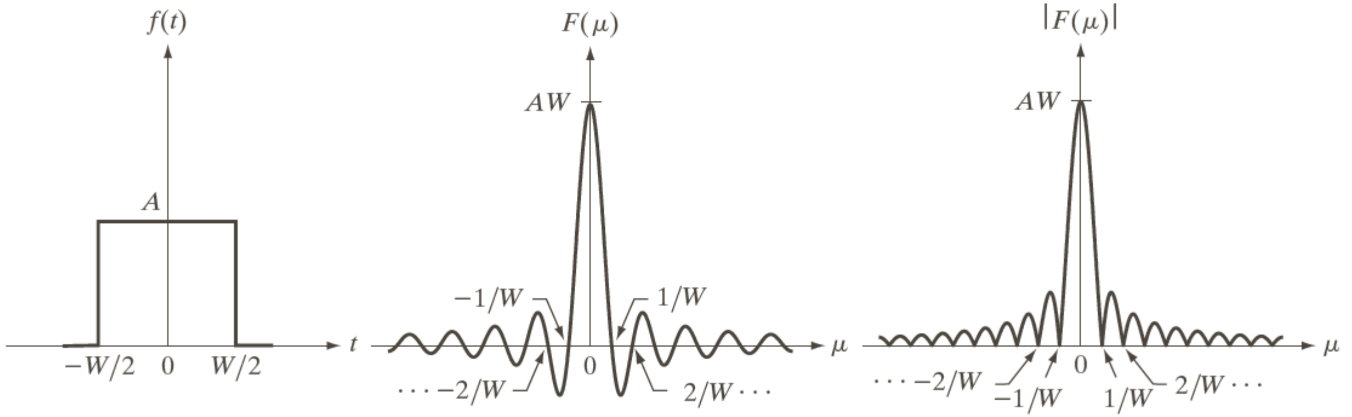

a b c

FIGURE 4.4 (a) A simple function; (b) its Fourier transform; and (c) the spectrum. All functions extend to infinity in both directions.

© 1992–2008 R. C. Gonzalez & R. E. Woods

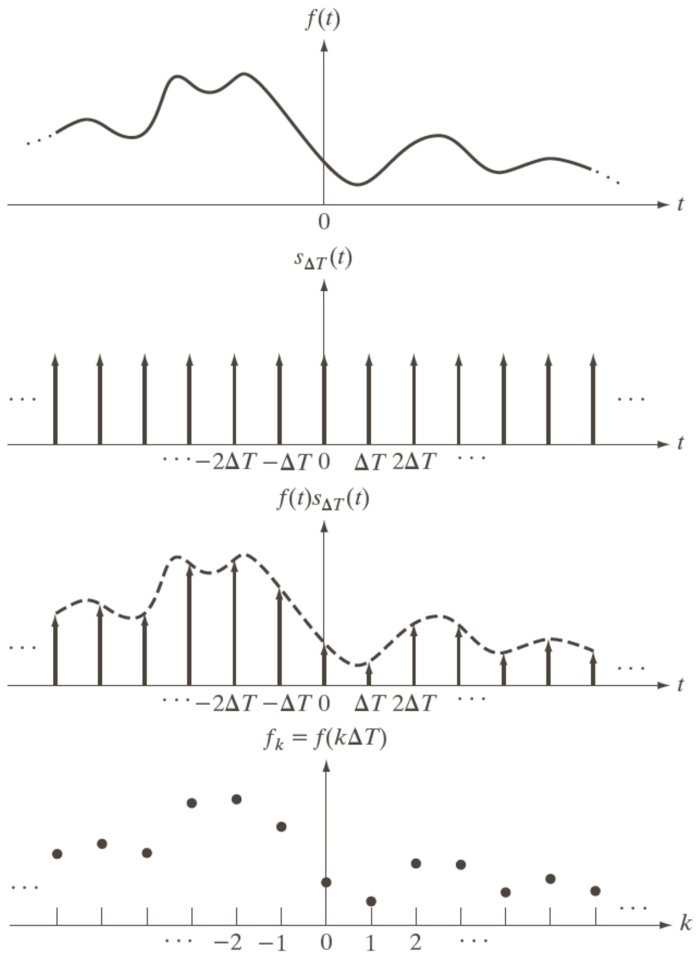

a
b
c
d

FIGURE 4.5 (a) A continuous function. (b) Train of impulses used to model the sampling process. (c) Sampled function formed as the product of (a) and (b). (d) Sample values obtained by integration and using the sifting property of the impulse. (The dashed line in (c) is shown for reference. It is not part of the data.)

© 1992–2008 R. C. Gonzalez & R. E. Woods

Chapter 4
Filtering in the Frequency Domain

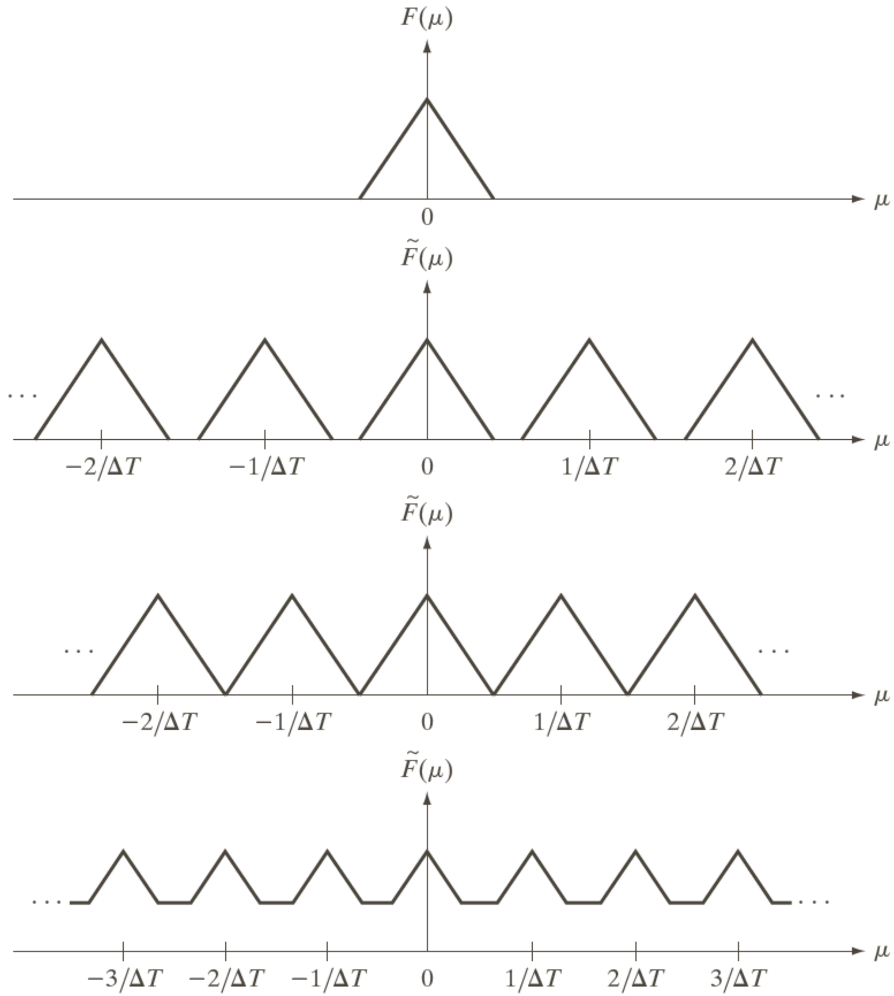

a
b
c
d

FIGURE 4.6 (a) Fourier transform of a band-limited function. (b)–(d) Transforms of the corresponding sampled function under the conditions of over-sampling, critically-sampling, and under-sampling, respectively.

© 1992–2008 R. C. Gonzalez & R. E. Woods

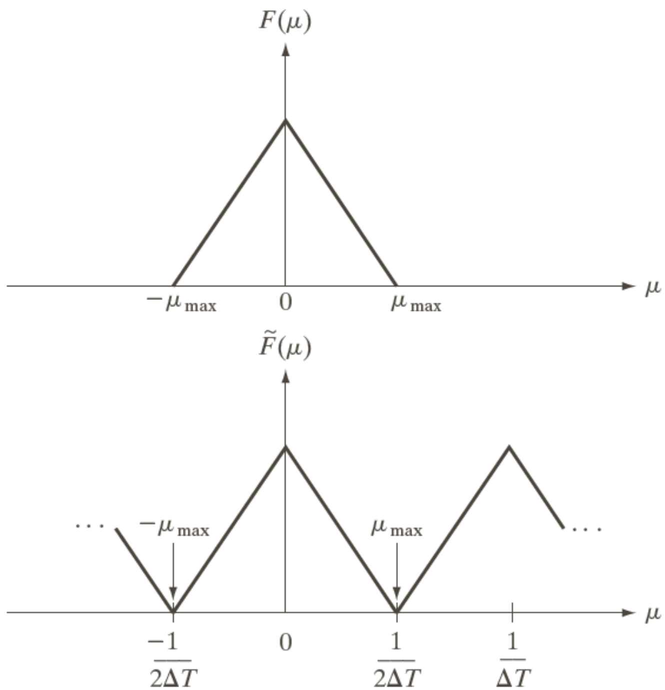

a
b

FIGURE 4.7 (a) Transform of a band-limited function. (b) Transform resulting from critically sampling the same function.

© 1992–2008 R. C. Gonzalez & R. E. Woods

Chapter 4
Filtering in the Frequency Domain

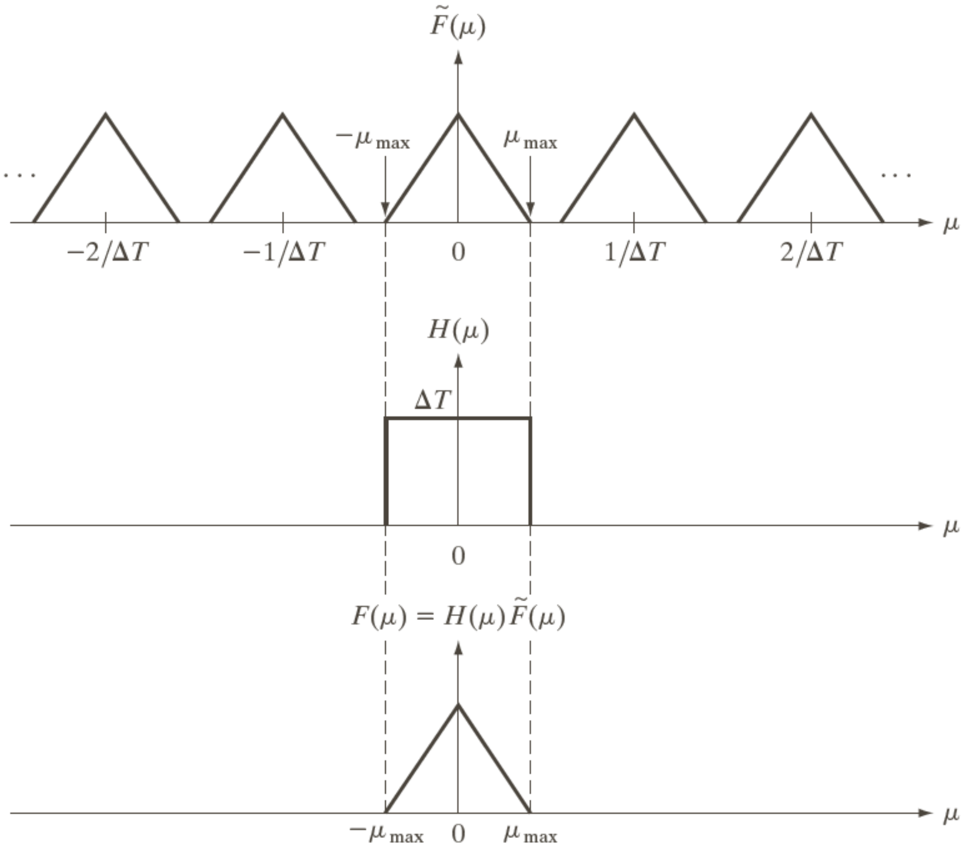

a
b
c

FIGURE 4.8 Extracting one period of the transform of a band-limited function using an ideal lowpass filter.

© 1992–2008 R. C. Gonzalez & R. E. Woods

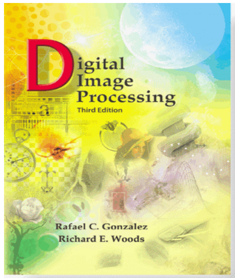

Chapter 4
Filtering in the Frequency Domain

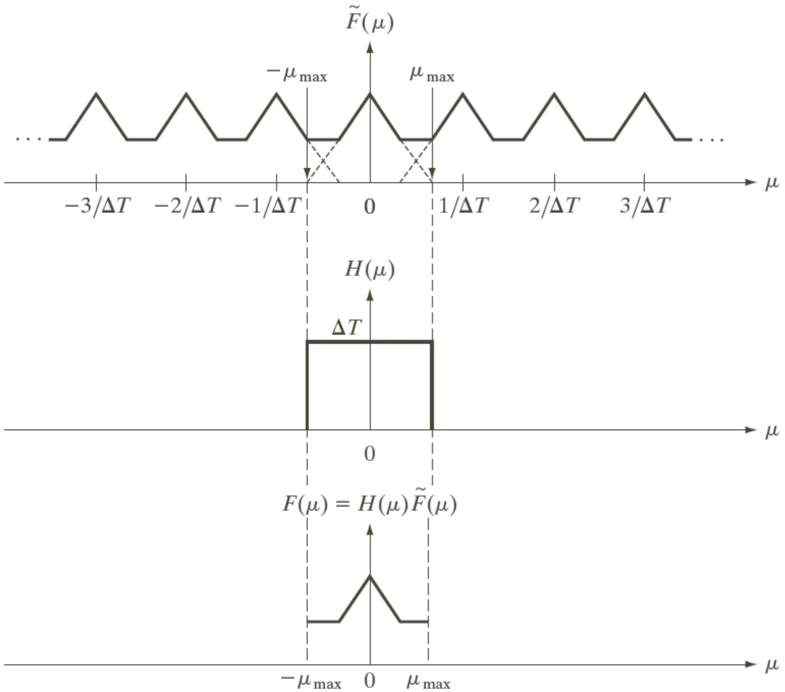

a
b
c

FIGURE 4.9 (a) Fourier transform of an under-sampled, band-limited function. (Interference from adjacent periods is shown dashed in this figure). (b) The same ideal lowpass filter used in Fig. 4.8(b). (c) The product of (a) and (b). The interference from adjacent periods results in aliasing that prevents perfect recovery of $F(\mu)$ and, therefore, of the original, band-limited continuous function. Compare with Fig. 4.8.

© 1992–2008 R. C. Gonzalez & R. E. Woods

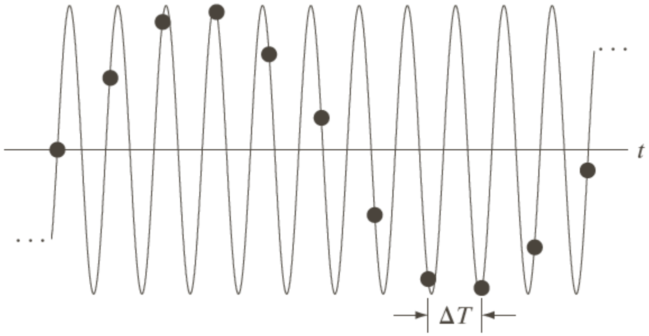

FIGURE 4.10 Illustration of aliasing. The under-sampled function (black dots) looks like a sine wave having a frequency much lower than the frequency of the continuous signal. The period of the sine wave is 2 s, so the zero crossings of the horizontal axis occur every second. ΔT is the separation between samples.

© 1992–2008 R. C. Gonzalez & R. E. Woods

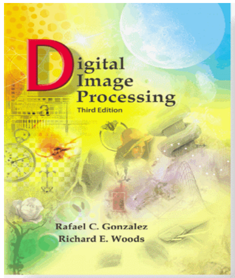

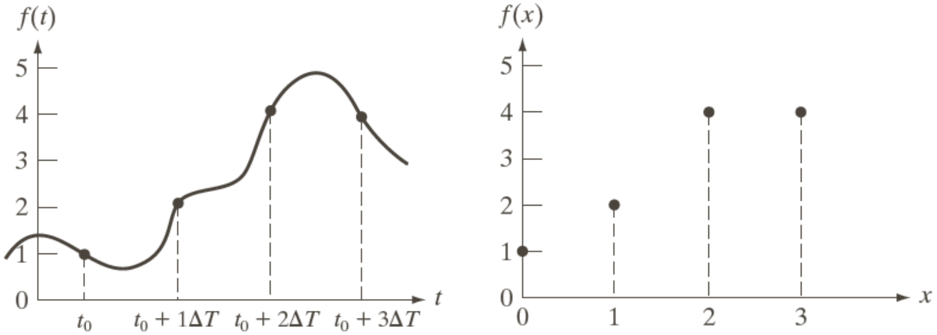

a b

FIGURE 4.11 (a) A function, and (b) samples in the x-domain. In (a), t is a continuous variable; in (b), x represents integer values.

© 1992–2008 R. C. Gonzalez & R. E. Woods

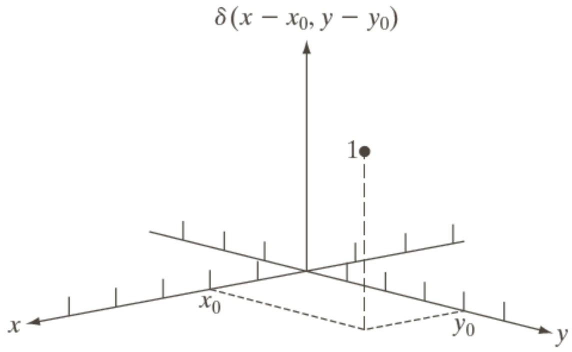

FIGURE 4.12 Two-dimensional unit discrete impulse. Variables x and y are discrete, and δ is zero everywhere except at coordinates (x_0, y_0).

© 1992–2008 R. C. Gonzalez & R. E. Woods

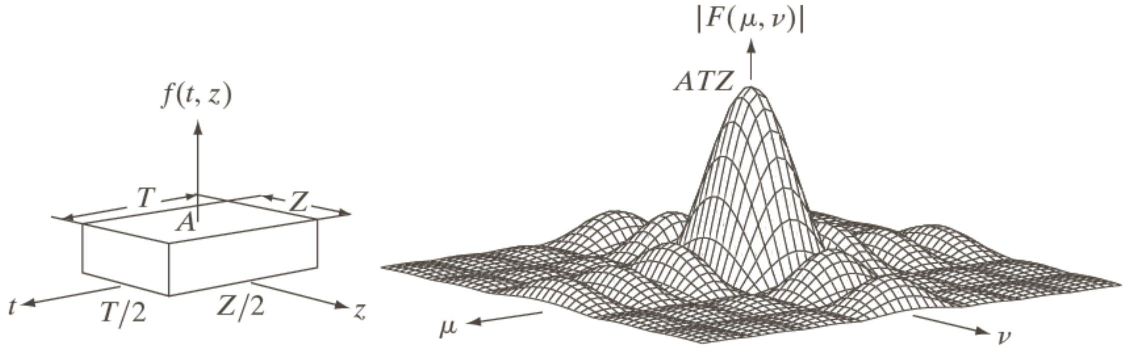

a b

FIGURE 4.13 (a) A 2-D function, and (b) a section of its spectrum (not to scale). The block is longer along the t-axis, so the spectrum is more "contracted" along the μ-axis. Compare with Fig. 4.4.

© 1992–2008 R. C. Gonzalez & R. E. Woods

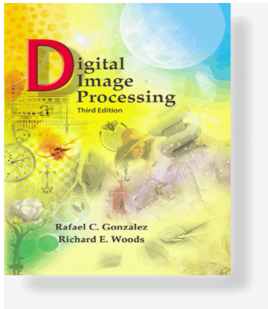

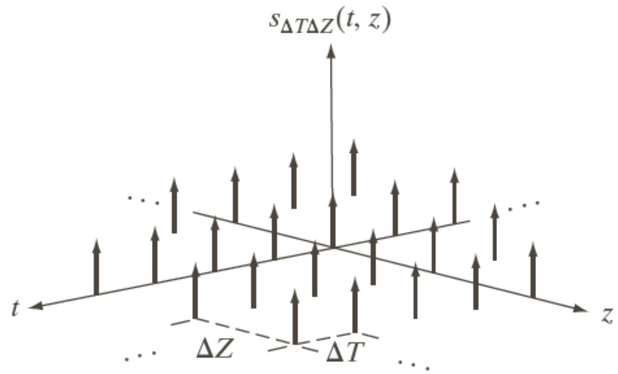

FIGURE 4.14 Two-dimensional impulse train.

© 1992–2008 R. C. Gonzalez & R. E. Woods

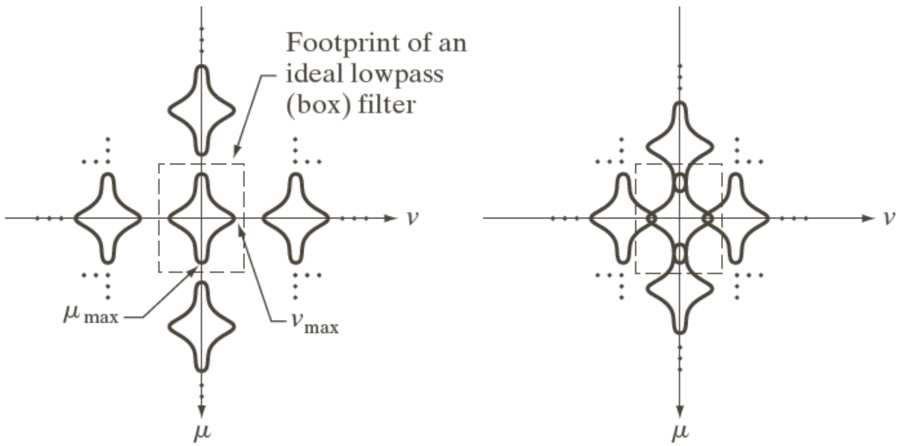

a b

FIGURE 4.15 Two-dimensional Fourier transforms of (a) an over-sampled, and (b) under-sampled band-limited function.

© 1992–2008 R. C. Gonzalez & R. E. Woods

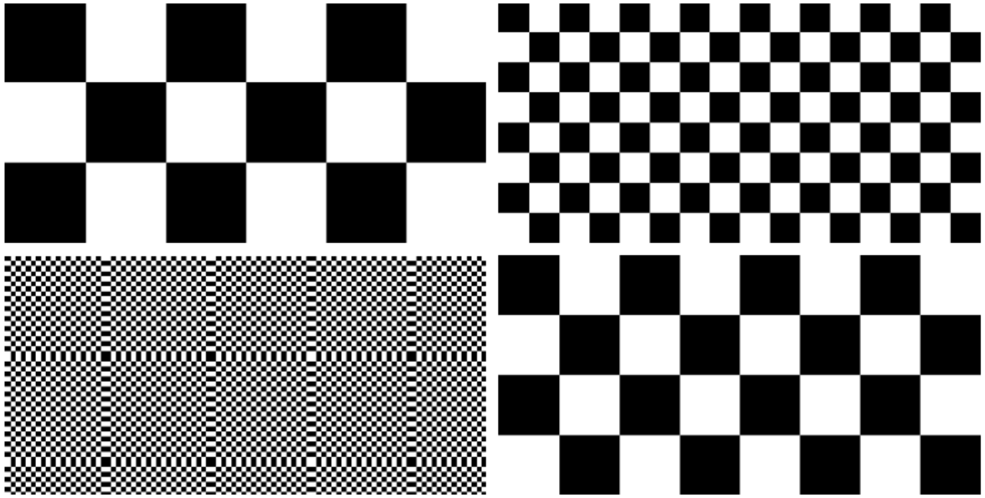

a	b
c	d

FIGURE 4.16 Aliasing in images. In (a) and (b), the lengths of the sides of the squares are 16 and 6 pixels, respectively, and aliasing is visually negligible. In (c) and (d), the sides of the squares are 0.9174 and 0.4798 pixels, respectively, and the results show significant aliasing. Note that (d) masquerades as a "normal" image.

© 1992–2008 R. C. Gonzalez & R. E. Woods

Chapter 4
Filtering in the Frequency Domain

a b c

FIGURE 4.17 Illustration of aliasing on resampled images. (a) A digital image with negligible visual aliasing. (b) Result of resizing the image to 50% of its original size by pixel deletion. Aliasing is clearly visible. (c) Result of blurring the image in (a) with a 3×3 averaging filter prior to resizing. The image is slightly more blurred than (b), but aliasing is not longer objectionable. (Original image courtesy of the Signal Compression Laboratory, University of California, Santa Barbara.)

© 1992–2008 R. C. Gonzalez & R. E. Woods

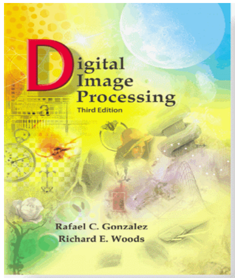

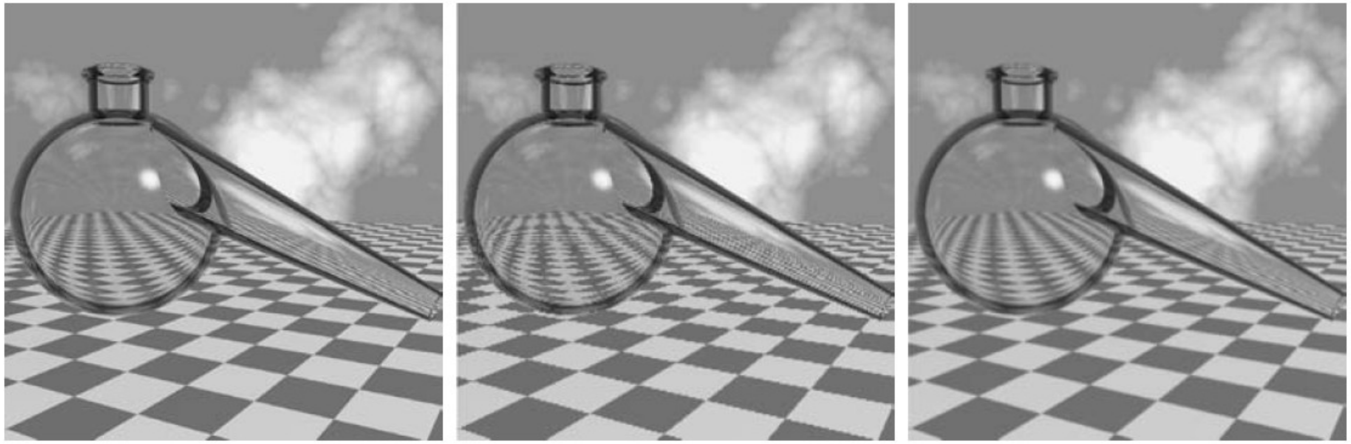

a b c

FIGURE 4.18 Illustration of jaggies. (a) A 1024 × 1024 digital image of a computer-generated scene with negligible visible aliasing. (b) Result of reducing (a) to 25% of its original size using bilinear interpolation. (c) Result of blurring the image in (a) with a 5 × 5 averaging filter prior to resizing it to 25% using bilinear interpolation. (Original image courtesy of D. P. Mitchell, Mental Landscape, LLC.)

© 1992–2008 R. C. Gonzalez & R. E. Woods

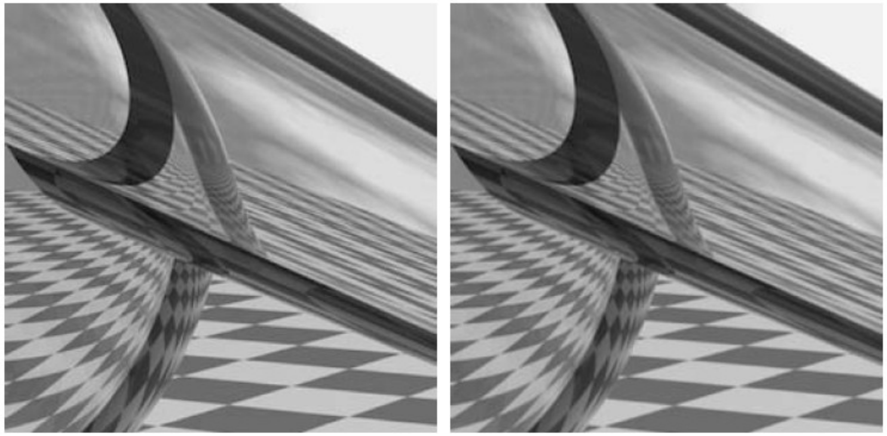

a b

FIGURE 4.19 Image zooming. (a) A 1024×1024 digital image generated by pixel replication from a 256×256 image extracted from the middle of Fig. 4.18(a). (b) Image generated using bi-linear interpolation, showing a significant reduction in jaggies.

© 1992–2008 R. C. Gonzalez & R. E. Woods

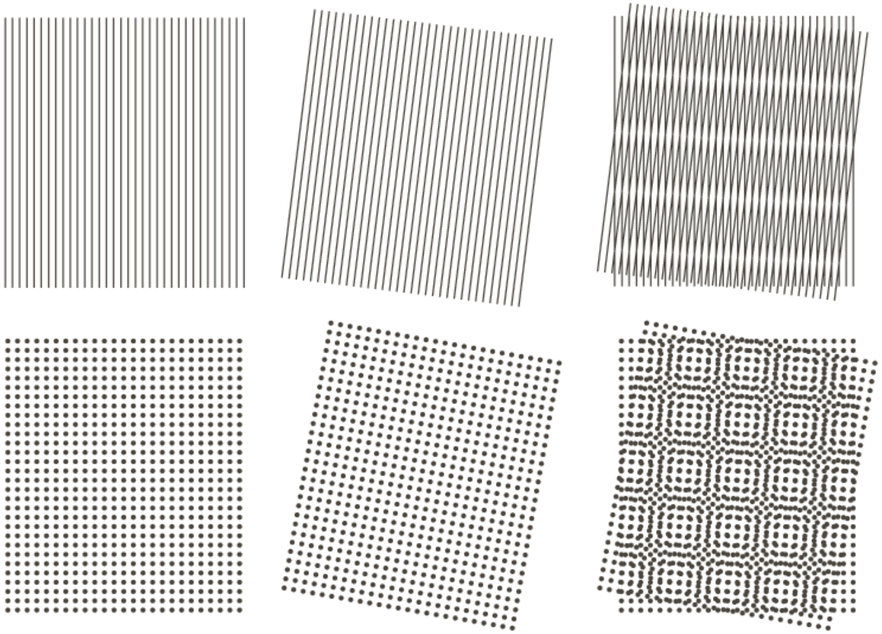

a	b	c
d	e	f

FIGURE 4.20 Examples of the moiré effect. These are ink drawings, not digitized patterns. Superimposing one pattern on the other is equivalent mathematically to multiplying the patterns.

© 1992–2008 R. C. Gonzalez & R. E. Woods

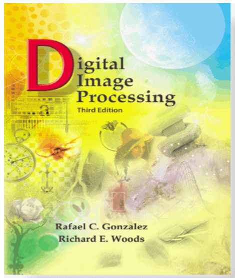

Chapter 4
Filtering in the Frequency Domain

FIGURE 4.21 A newspaper image of size 246×168 pixels sampled at 75 dpi showing a moiré pattern. The moiré pattern in this image is the interference pattern created between the $\pm 45°$ orientation of the halftone dots and the north–south orientation of the sampling grid used to digitize the image.

© 1992–2008 R. C. Gonzalez & R. E. Woods

Chapter 4
Filtering in the Frequency Domain

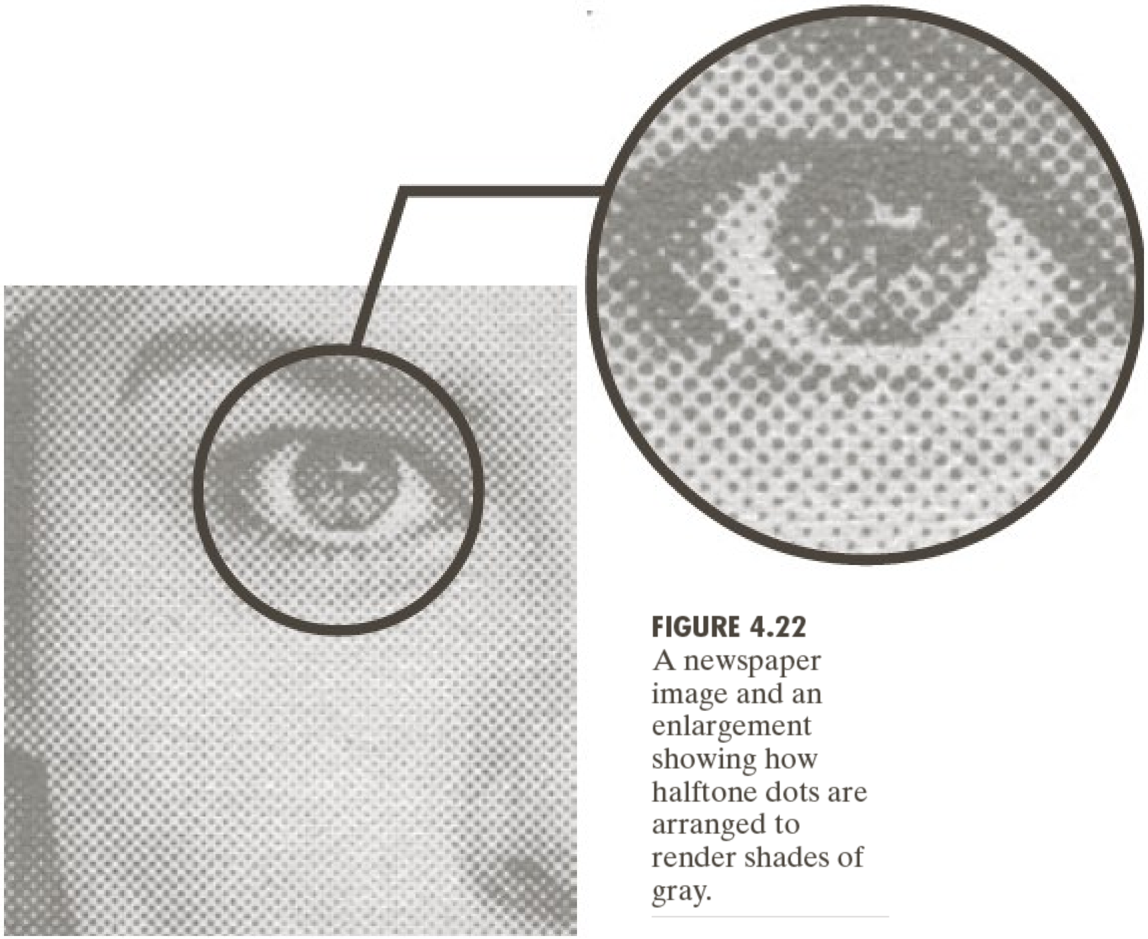

FIGURE 4.22
A newspaper image and an enlargement showing how halftone dots are arranged to render shades of gray.

© 1992–2008 R. C. Gonzalez & R. E. Woods

Chapter 4
Filtering in the Frequency Domain

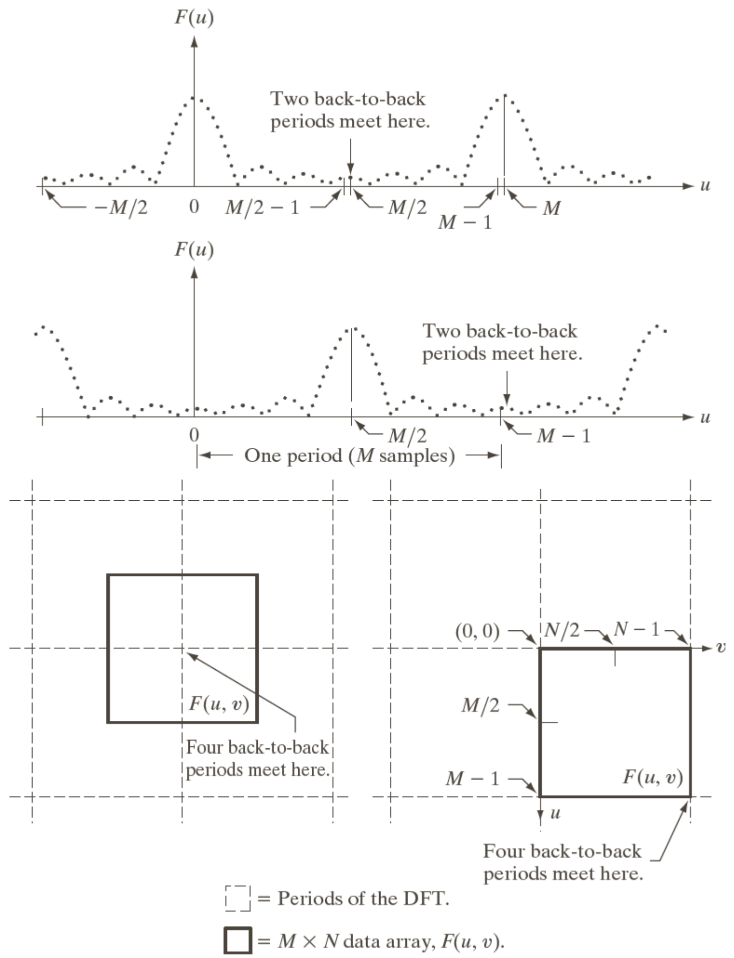

a
b
c d

FIGURE 4.23 Centering the Fourier transform. (a) A 1-D DFT showing an infinite number of periods. (b) Shifted DFT obtained by multiplying $f(x)$ by $(-1)^x$ before computing $F(u)$. (c) A 2-D DFT showing an infinite number of periods. The solid area is the $M \times N$ data array, $F(u, v)$, obtained with Eq. (4.5-15). This array consists of four quarter periods. (d) A Shifted DFT obtained by multiplying $f(x, y)$ by $(-1)^{x+y}$ before computing $F(u, v)$. The data now contains one complete, centered period, as in (b).

© 1992–2008 R. C. Gonzalez & R. E. Woods

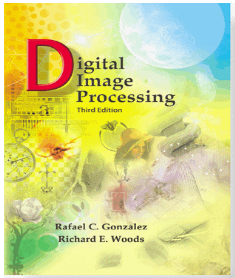

Chapter 4
Filtering in the Frequency Domain

	Spatial Domain[†]		Frequency Domain[†]
1)	$f(x, y)$ real	$\Leftrightarrow$	$F^*(u, v) = F(-u, -v)$
2)	$f(x, y)$ imaginary	$\Leftrightarrow$	$F^*(-u, -v) = -F(u, v)$
3)	$f(x, y)$ real	$\Leftrightarrow$	$R(u, v)$ even; $I(u, v)$ odd
4)	$f(x, y)$ imaginary	$\Leftrightarrow$	$R(u, v)$ odd; $I(u, v)$ even
5)	$f(-x, -y)$ real	$\Leftrightarrow$	$F^*(u, v)$ complex
6)	$f(-x, -y)$ complex	$\Leftrightarrow$	$F(-u, -v)$ complex
7)	$f^*(x, y)$ complex	$\Leftrightarrow$	$F^*(-u - v)$ complex
8)	$f(x, y)$ real and even	$\Leftrightarrow$	$F(u, v)$ real and even
9)	$f(x, y)$ real and odd	$\Leftrightarrow$	$F(u, v)$ imaginary and odd
10)	$f(x, y)$ imaginary and even	$\Leftrightarrow$	$F(u, v)$ imaginary and even
11)	$f(x, y)$ imaginary and odd	$\Leftrightarrow$	$F(u, v)$ real and odd
12)	$f(x, y)$ complex and even	$\Leftrightarrow$	$F(u, v)$ complex and even
13)	$f(x, y)$ complex and odd	$\Leftrightarrow$	$F(u, v)$ complex and odd

[†]Recall that x, y, u, and v are *discrete* (integer) variables, with x and u in the range $[0, M - 1]$, and y, and v in the range $[0, N - 1]$. To say that a complex function is *even* means that its real *and* imaginary parts are even, and similarly for an odd complex function.

TABLE 4.1 Some symmetry properties of the 2-D DFT and its inverse. $R(u, v)$ and $I(u, v)$ are the real and imaginary parts of $F(u, v)$, respectively. The term *complex* indicates that a function has nonzero real and imaginary parts.

© 1992–2008 R. C. Gonzalez & R. E. Woods

Chapter 4
Filtering in the Frequency Domain

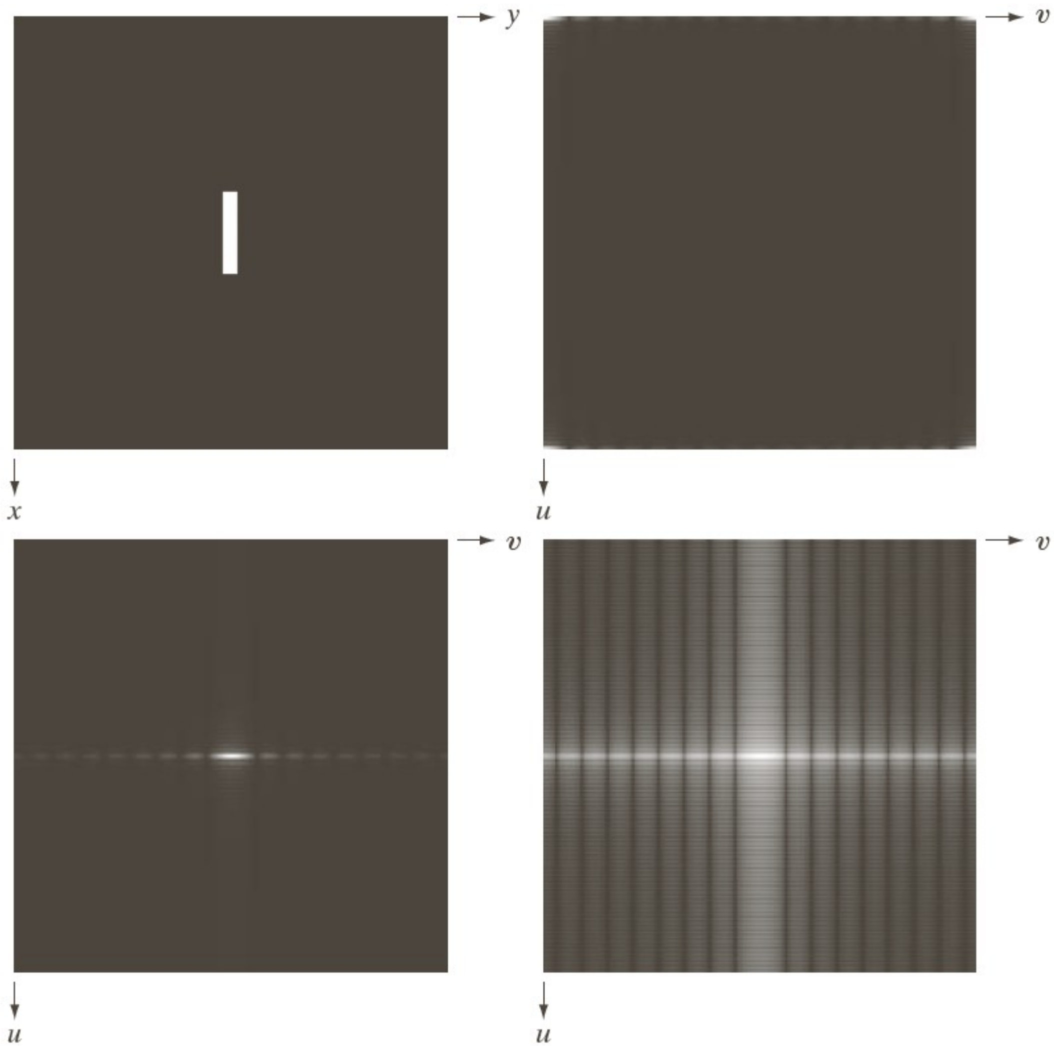

a b
c d

FIGURE 4.24 (a) Image. (b) Spectrum showing bright spots in the four corners. (c) Centered spectrum. (d) Result showing increased detail after a log transformation. The zero crossings of the spectrum are closer in the vertical direction because the rectangle in (a) is longer in that direction. The coordinate convention used throughout the book places the origin of the spatial and frequency domains at the top left.

© 1992–2008 R. C. Gonzalez & R. E. Woods

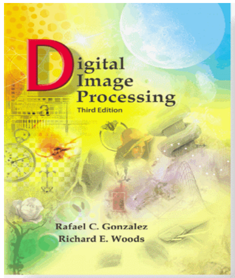

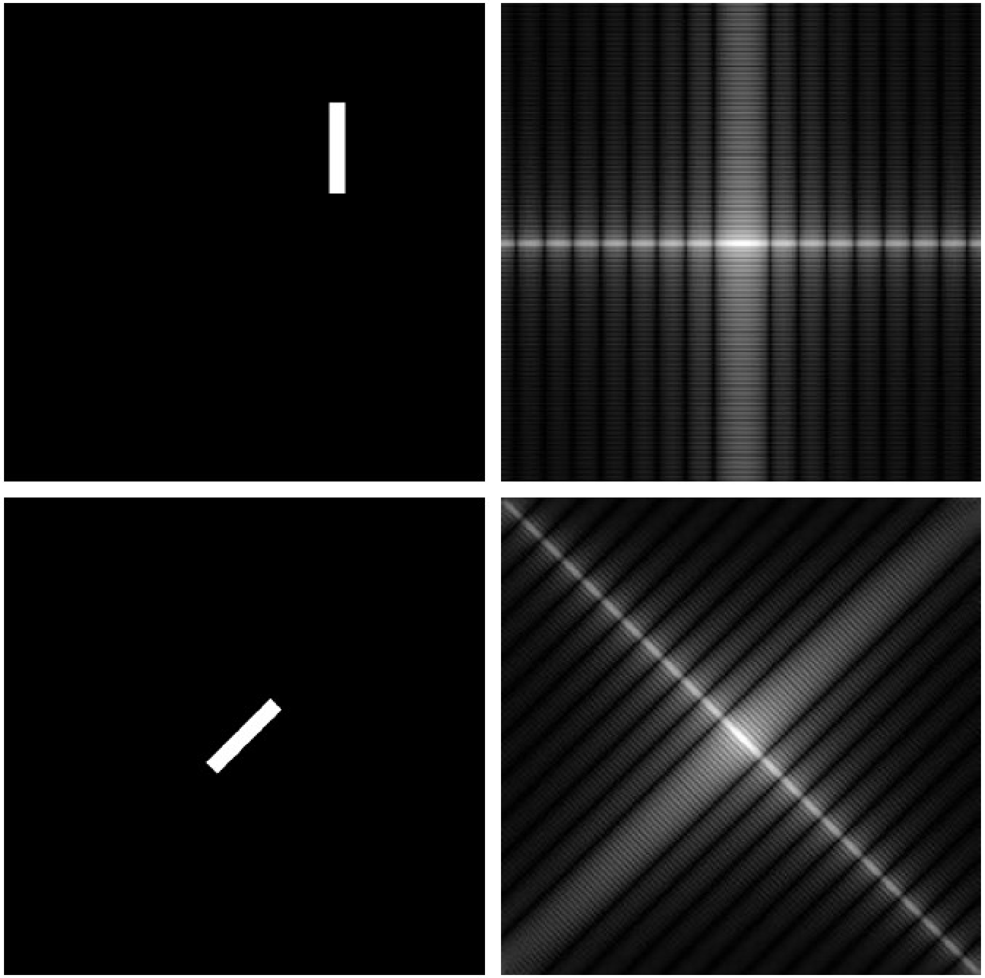

a b
c d

FIGURE 4.25 (a) The rectangle in Fig. 4.24(a) translated, and (b) the corresponding spectrum. (c) Rotated rectangle, and (d) the corresponding spectrum. The spectrum corresponding to the translated rectangle is identical to the spectrum corresponding to the original image in Fig. 4.24(a).

© 1992–2008 R. C. Gonzalez & R. E. Woods

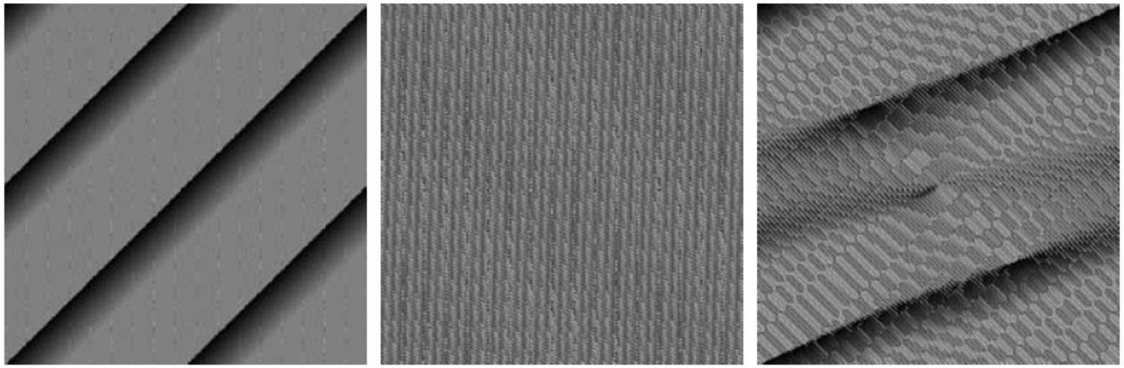

a b c

FIGURE 4.26 Phase angle array corresponding (a) to the image of the centered rectangle in Fig. 4.24(a), (b) to the translated image in Fig. 4.25(a), and (c) to the rotated image in Fig. 4.25(c).

© 1992–2008 R. C. Gonzalez & R. E. Woods

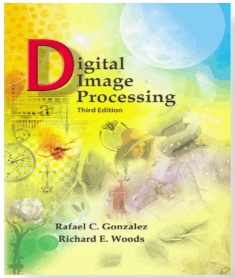

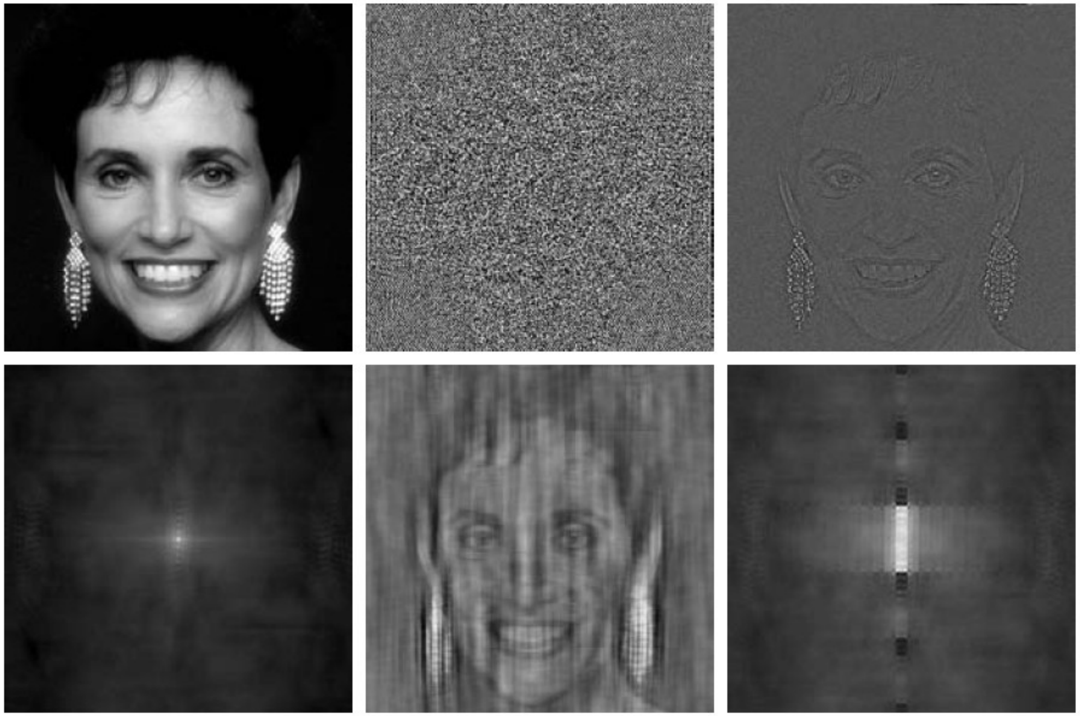

a b c
d e f

FIGURE 4.27 (a) Woman. (b) Phase angle. (c) Woman reconstructed using only the phase angle. (d) Woman reconstructed using only the spectrum. (e) Reconstruction using the phase angle corresponding to the woman and the spectrum corresponding to the rectangle in Fig. 4.24(a). (f) Reconstruction using the phase of the rectangle and the spectrum of the woman.

© 1992–2008 R. C. Gonzalez & R. E. Woods

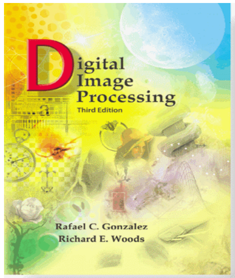

Chapter 4
Filtering in the Frequency Domain

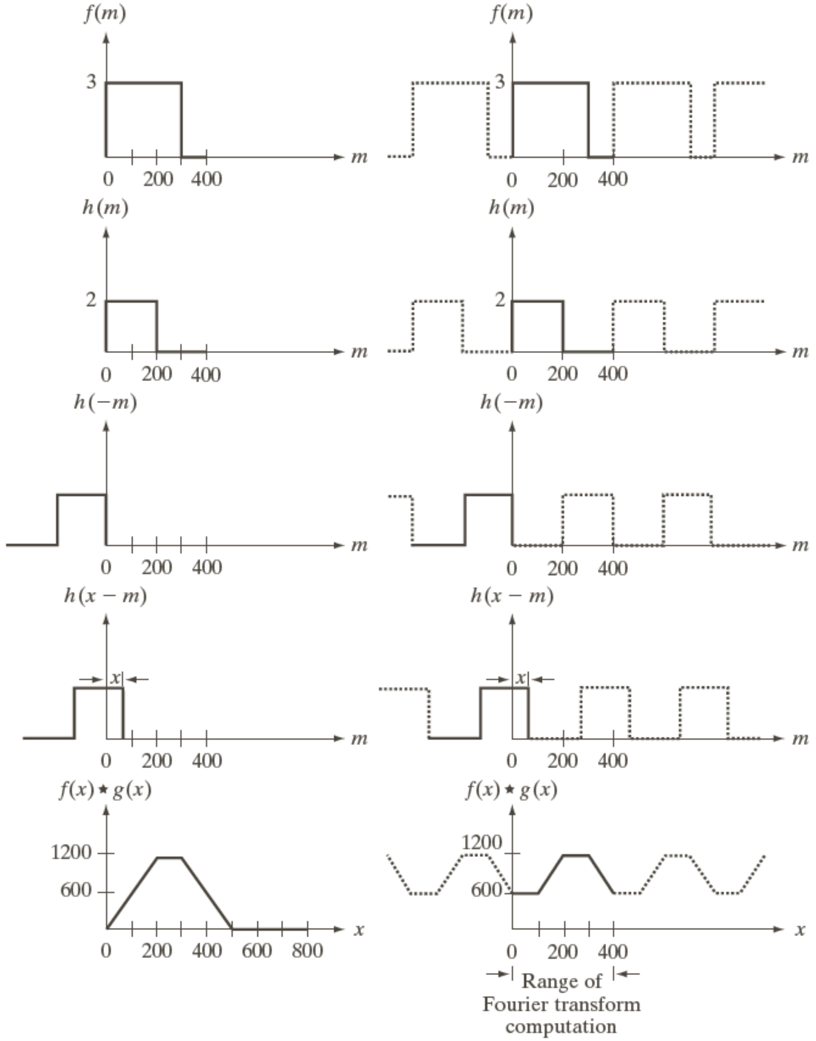

FIGURE 4.28 Left column: convolution of two discrete functions obtained using the approach discussed in Section 3.4.2. The result in (e) is correct. Right column: Convolution of the same functions, but taking into account the periodicity implied by the DFT. Note in (j) how data from adjacent periods produce wraparound error, yielding an incorrect convolution result. To obtain the correct result, function padding must be used.

© 1992–2008 R. C. Gonzalez & R. E. Woods

TABLE 4.2 Summary of DFT definitions and corresponding expressions.

Name	Expression(s)
1) Discrete Fourier transform (DFT) of $f(x, y)$	$F(u, v) = \sum_{x=0}^{M-1} \sum_{y=0}^{N-1} f(x, y) e^{-j2\pi(ux/M + vy/N)}$
2) Inverse discrete Fourier transform (IDFT) of $F(u, v)$	$f(x, y) = \frac{1}{MN} \sum_{u=0}^{M-1} \sum_{v=0}^{N-1} F(u, v) e^{j2\pi(ux/M + vy/N)}$
3) Polar representation	$F(u, v) = \lvert F(u, v)\rvert e^{j\phi(u,v)}$
4) Spectrum	$\lvert F(u, v)\rvert = \left[R^2(u, v) + I^2(u, v)\right]^{1/2}$ $R = \text{Real}(F); \quad I = \text{Imag}(F)$
5) Phase angle	$\phi(u, v) = \tan^{-1}\left[\frac{I(u, v)}{R(u, v)}\right]$
6) Power spectrum	$P(u, v) = \lvert F(u, v)\rvert^2$
7) Average value	$\overline{f}(x, y) = \frac{1}{MN} \sum_{x=0}^{M-1} \sum_{y=0}^{N-1} f(x, y) = \frac{1}{MN} F(0, 0)$

(*Continued*)

© 1992–2008 R. C. Gonzalez & R. E. Woods

Chapter 4
Filtering in the Frequency Domain

TABLE 4.2 (*Continued*)

Name	Expression(s)
8) Periodicity (k_1 and k_2 are integers)	$F(u,v) = F(u + k_1M, v) = F(u, v + k_2N)$ $= F(u + k_1M, v + k_2N)$ $f(x,y) = f(x + k_1M, y) = f(x, y + k_2N)$ $= f(x + k_1M, y + k_2N)$
9) Convolution	$f(x,y) \bigstar h(x,y) = \sum_{m=0}^{M-1}\sum_{n=0}^{N-1} f(m,n)h(x-m, y-n)$
10) Correlation	$f(x,y) \star h(x,y) = \sum_{m=0}^{M-1}\sum_{n=0}^{N-1} f^*(m,n)h(x+m, y+n)$
11) Separability	The 2-D DFT can be computed by computing 1-D DFT transforms along the rows (columns) of the image, followed by 1-D transforms along the columns (rows) of the result. See Section 4.11.1.
12) Obtaining the inverse Fourier transform using a forward transform algorithm.	$MNf^*(x,y) = \sum_{u=0}^{M-1}\sum_{v=0}^{N-1} F^*(u,v)e^{-j2\pi(ux/M + vy/N)}$ This equation indicates that inputting $F^*(u,v)$ into an algorithm that computes the forward transform (right side of above equation) yields $MNf^*(x,y)$. Taking the complex conjugate and dividing by MN gives the desired inverse. See Section 4.11.2.

© 1992–2008 R. C. Gonzalez & R. E. Woods

Name	DFT Pairs
1) Symmetry properties	See Table 4.1
2) Linearity	$af_1(x, y) + bf_2(x, y) \Leftrightarrow aF_1(u, v) + bF_2(u, v)$
3) Translation (general)	$f(x, y)e^{j2\pi(u_0x/M+v_0y/N)} \Leftrightarrow F(u - u_0, v - v_0)$ $f(x - x_0, y - y_0) \Leftrightarrow F(u, v)e^{-j2\pi(ux_0/M+vy_0/N)}$
4) Translation to center of the frequency rectangle, $(M/2, N/2)$	$f(x, y)(-1)^{x+y} \Leftrightarrow F(u - M/2, v - N/2)$ $f(x - M/2, y - N/2) \Leftrightarrow F(u, v)(-1)^{u+v}$
5) Rotation	$f(r, \theta + \theta_0) \Leftrightarrow F(\omega, \varphi + \theta_0)$ $x = r\cos\theta \quad y = r\sin\theta \quad u = \omega\cos\varphi \quad v = \omega\sin\varphi$
6) Convolution theorem†	$f(x, y) \star h(x, y) \Leftrightarrow F(u, v)H(u, v)$ $f(x, y)h(x, y) \Leftrightarrow F(u, v) \star H(u, v)$

(Continued)

TABLE 4.3 Summary of DFT pairs. The closed-form expressions in 12 and 13 are valid only for continuous variables. They can be used with discrete variables by sampling the closed-form, continuous expressions.

© 1992–2008 R. C. Gonzalez & R. E. Woods

TABLE 4.3
(Continued)

Name	DFT Pairs
7) Correlation theorem[†]	$f(x, y) \star h(x, y) \Leftrightarrow F^*(u, v)\, H(u, v)$ $f^*(x, y) h(x, y) \Leftrightarrow F(u, v) \star H(u, v)$
8) Discrete unit impulse	$\delta(x, y) \Leftrightarrow 1$
9) Rectangle	$\text{rect}[a, b] \Leftrightarrow ab \dfrac{\sin(\pi ua)}{(\pi ua)} \dfrac{\sin(\pi vb)}{(\pi vb)} e^{-j\pi(ua+vb)}$
10) Sine	$\sin(2\pi u_0 x + 2\pi v_0 y) \Leftrightarrow$ $j\dfrac{1}{2}\left[\delta(u + Mu_0, v + Nv_0) - \delta(u - Mu_0, v - Nv_0)\right]$
11) Cosine	$\cos(2\pi u_0 x + 2\pi v_0 y) \Leftrightarrow$ $\dfrac{1}{2}\left[\delta(u + Mu_0, v + Nv_0) + \delta(u - Mu_0, v - Nv_0)\right]$
The following Fourier transform pairs are derivable only for continuous variables, denoted as before by t and z for spatial variables and by μ and ν for frequency variables. These results can be used for DFT work by sampling the continuous forms.	
12) *Differentiation* (The expressions on the right assume that $f(\pm\infty, \pm\infty) = 0$.)	$\left(\dfrac{\partial}{\partial t}\right)^m \left(\dfrac{\partial}{\partial z}\right)^n f(t, z) \Leftrightarrow (j2\pi\mu)^m (j2\pi\nu)^n F(\mu, \nu)$ $\dfrac{\partial^m f(t, z)}{\partial t^m} \Leftrightarrow (j2\pi\mu)^m F(\mu, \nu); \dfrac{\partial^n f(t, z)}{\partial z^n} \Leftrightarrow (j2\pi\nu)^n F(\mu, \nu)$
13) *Gaussian*	$A2\pi\sigma^2 e^{-2\pi^2\sigma^2(t^2+z^2)} \Leftrightarrow Ae^{-(\mu^2+\nu^2)/2\sigma^2}$ (A is a constant)

[†]Assumes that the functions have been extended by zero padding. Convolution and correlation are associative, commutative, and distributive.

© 1992–2008 R. C. Gonzalez & R. E. Woods

Chapter 4
Filtering in the Frequency Domain

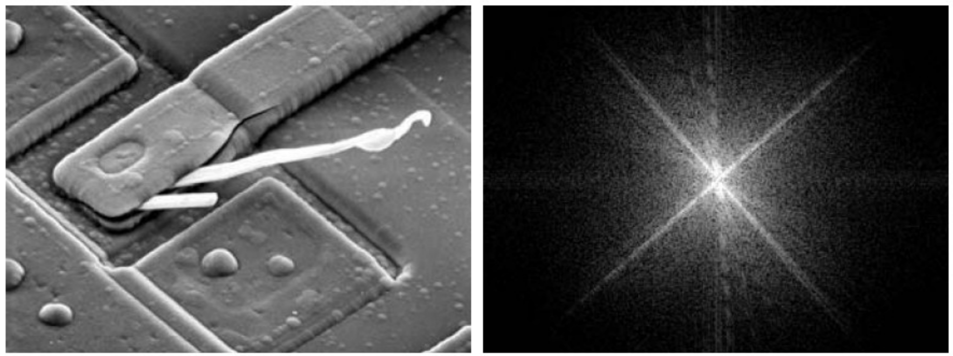

a b

FIGURE 4.29 (a) SEM image of a damaged integrated circuit. (b) Fourier spectrum of (a). (Original image courtesy of Dr. J. M. Hudak, Brockhouse Institute for Materials Research, McMaster University, Hamilton, Ontario, Canada.)

© 1992–2008 R. C. Gonzalez & R. E. Woods

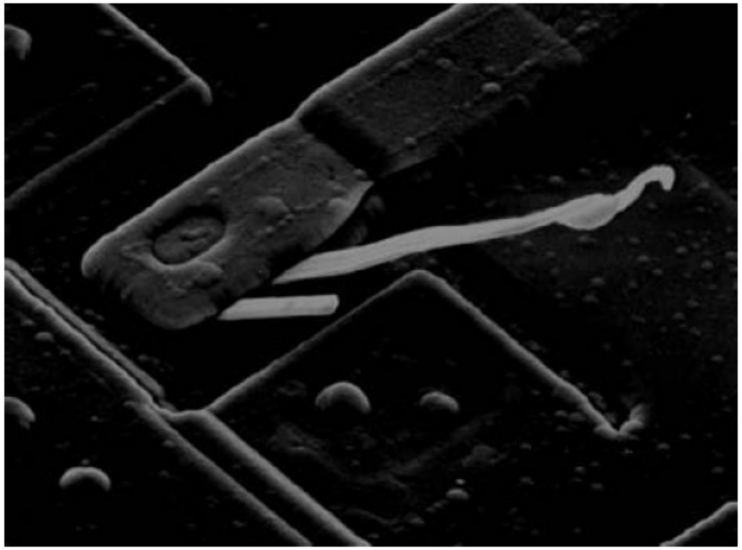

FIGURE 4.30 Result of filtering the image in Fig. 4.29(a) by setting to 0 the term $F(M/2, N/2)$ in the Fourier transform.

© 1992–2008 R. C. Gonzalez & R. E. Woods

Chapter 4
Filtering in the Frequency Domain

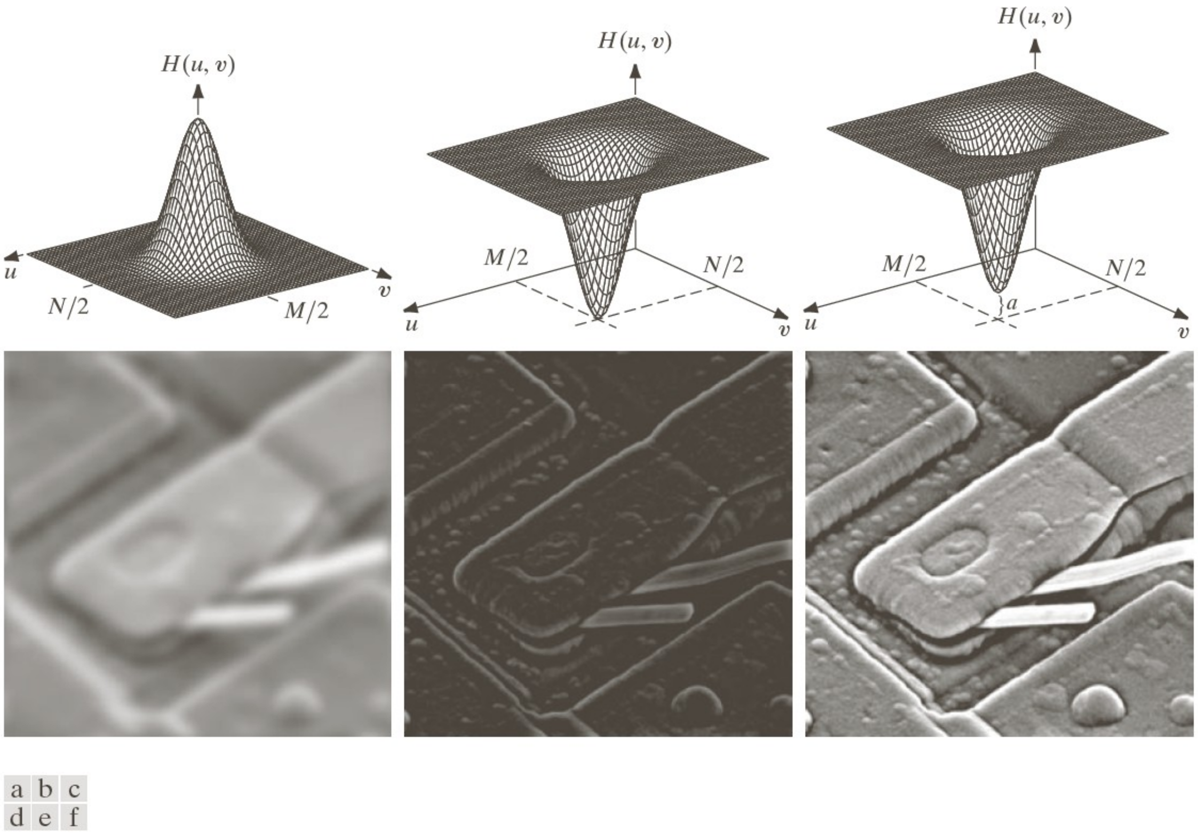

FIGURE 4.31 Top row: frequency domain filters. Bottom row: corresponding filtered images obtained using Eq. (4.7-1). We used $a = 0.85$ in (c) to obtain (f) (the height of the filter itself is 1). Compare (f) with Fig. 4.29(a).

© 1992–2008 R. C. Gonzalez & R. E. Woods

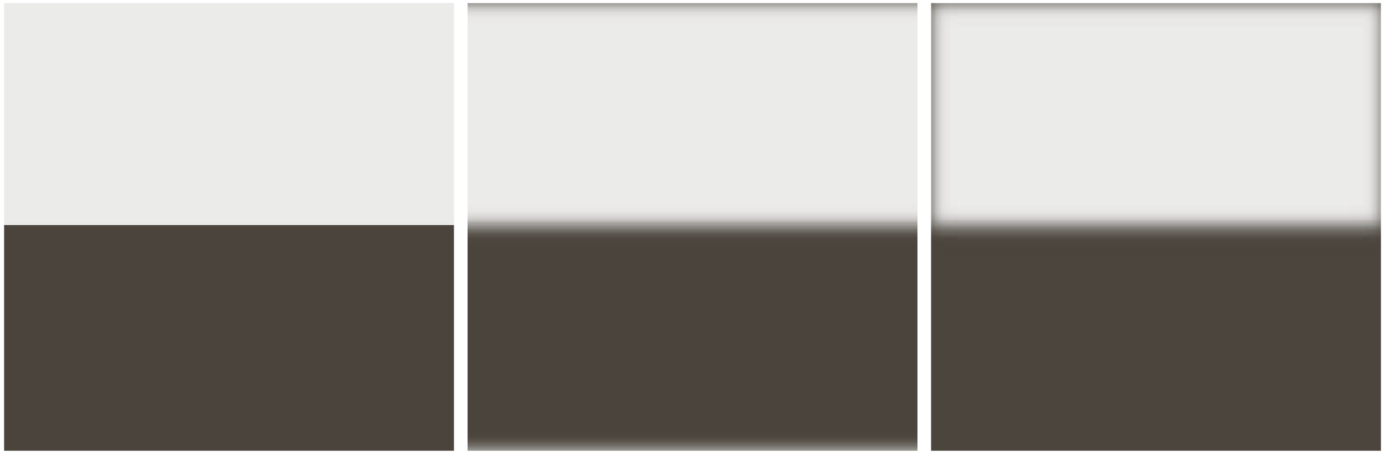

a b c

FIGURE 4.32 (a) A simple image. (b) Result of blurring with a Gaussian lowpass filter without padding. (c) Result of lowpass filtering with padding. Compare the light area of the vertical edges in (b) and (c).

© 1992–2008 R. C. Gonzalez & R. E. Woods

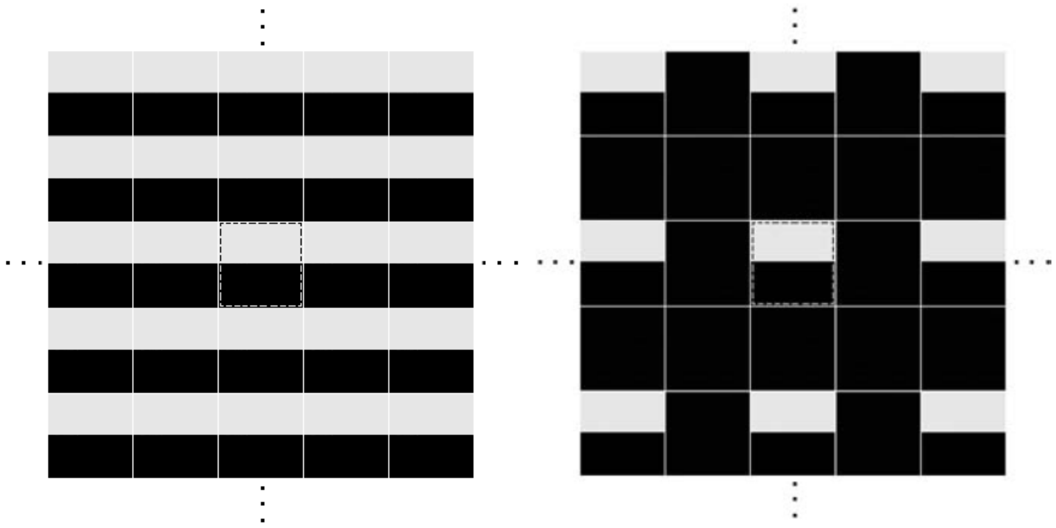

a b

FIGURE 4.33 2-D image periodicity inherent in using the DFT. (a) Periodicity without image padding. (b) Periodicity after padding with 0s (black). The dashed areas in the center correspond to the image in Fig. 4.32(a). (The thin white lines in both images are superimposed for clarity; they are not part of the data.)

© 1992–2008 R. C. Gonzalez & R. E. Woods

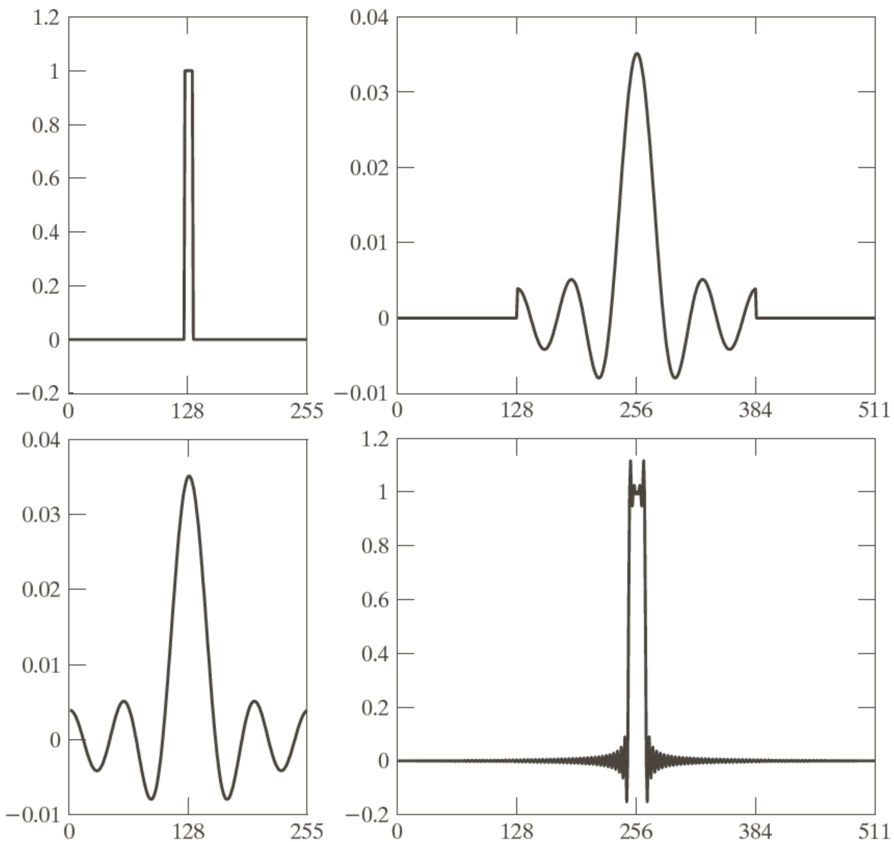

a c
b d

FIGURE 4.34
(a) Original filter specified in the (centered) frequency domain. (b) Spatial representation obtained by computing the IDFT of (a). (c) Result of padding (b) to twice its length (note the discontinuities). (d) Corresponding filter in the frequency domain obtained by computing the DFT of (c). Note the ringing caused by the discontinuities in (c). (The curves appear continuous because the points were joined to simplify visual analysis.)

© 1992–2008 R. C. Gonzalez & R. E. Woods

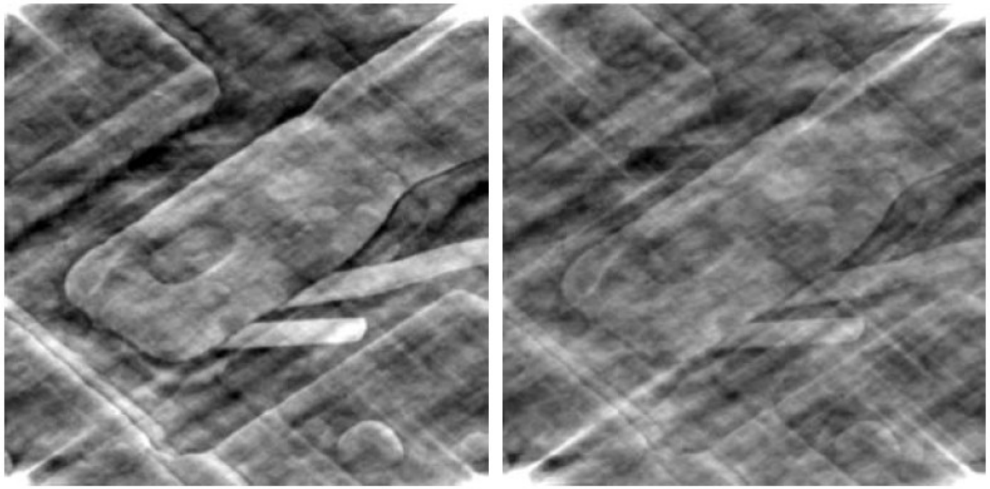

a b

FIGURE 4.35 (a) Image resulting from multiplying by 0.5 the phase angle in Eq. (4.6-15) and then computing the IDFT. (b) The result of multiplying the phase by 0.25. The spectrum was not changed in either of the two cases.

© 1992–2008 R. C. Gonzalez & R. E. Woods

Chapter 4
Filtering in the Frequency Domain

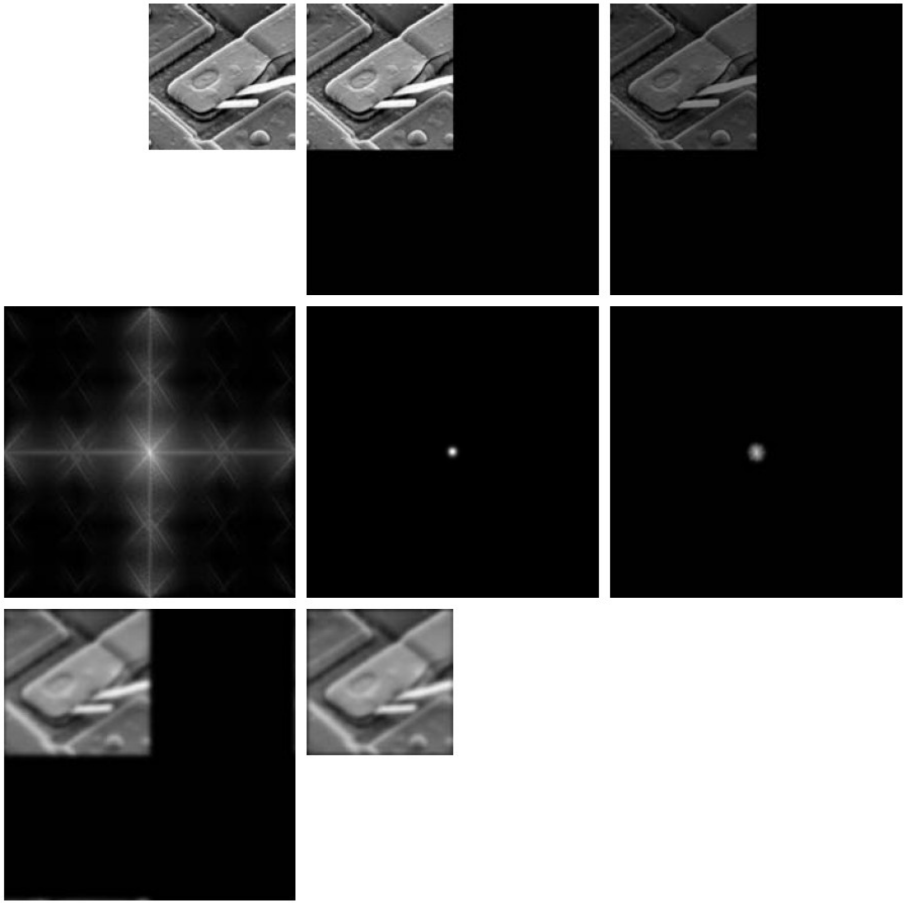

a b c
d e f
g h

FIGURE 4.36 (a) An $M \times N$ image, f. (b) Padded image, f_p of size $P \times Q$. (c) Result of multiplying f_p by $(-1)^{x+y}$. (d) Spectrum of F_p. (e) Centered Gaussian lowpass filter, H, of size $P \times Q$. (f) Spectrum of the product HF_p. (g) g_p, the product of $(-1)^{x+y}$ and the real part of the IDFT of HF_p. (h) Final result, g, obtained by cropping the first M rows and N columns of g_p.

© 1992–2008 R. C. Gonzalez & R. E. Woods

Chapter 4
Filtering in the Frequency Domain

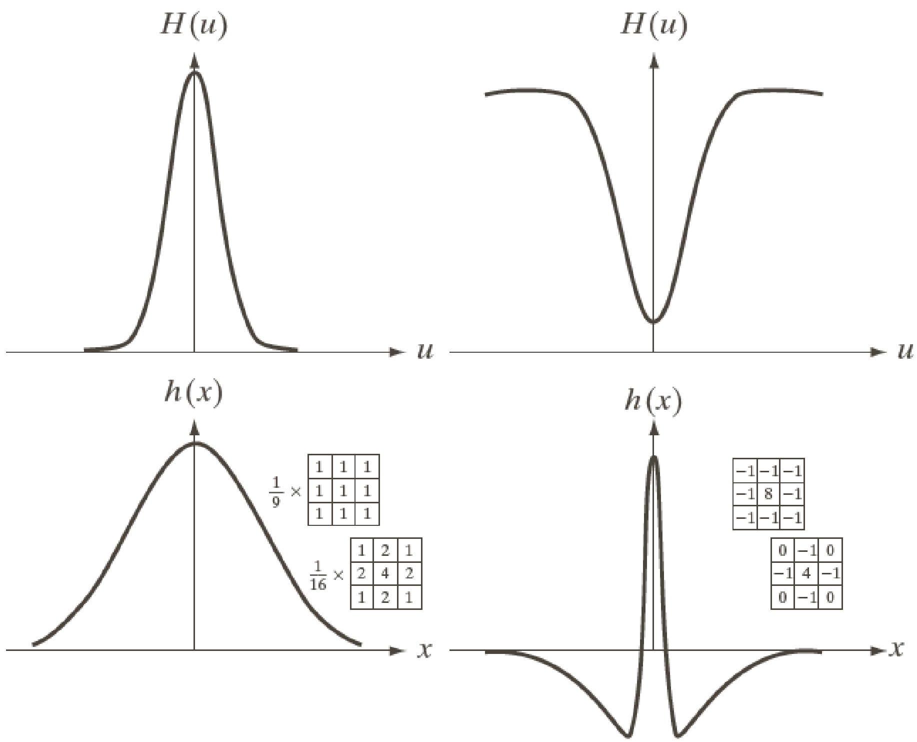

a c
b d

FIGURE 4.37 (a) A 1-D Gaussian lowpass filter in the frequency domain. (b) Spatial lowpass filter corresponding to (a). (c) Gaussian highpass filter in the frequency domain. (d) Spatial highpass filter corresponding to (c). The small 2-D masks shown are spatial filters we used in Chapter 3.

© 1992–2008 R. C. Gonzalez & R. E. Woods

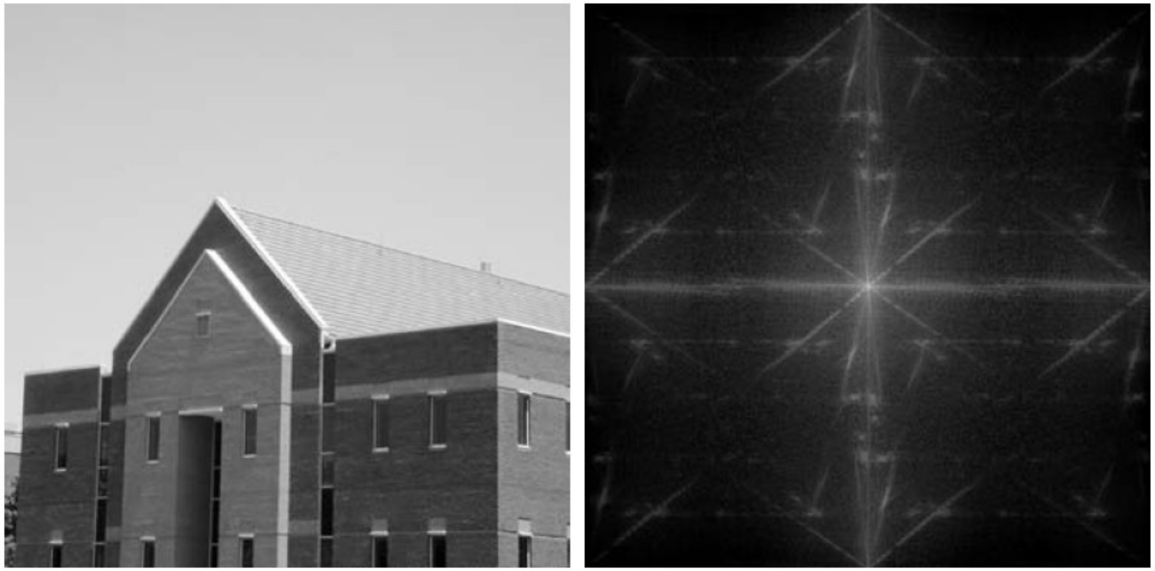

a b

FIGURE 4.38 (a) Image of a building, and (b) its spectrum.

© 1992–2008 R. C. Gonzalez & R. E. Woods

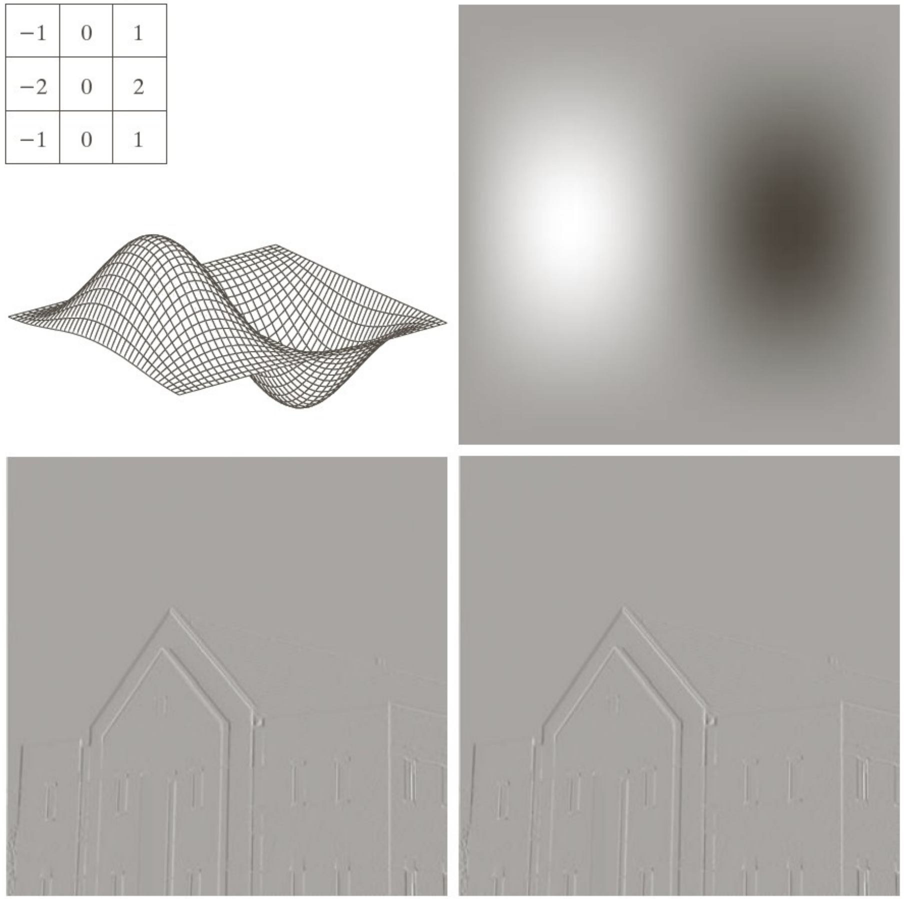

−1	0	1
−2	0	2
−1	0	1

a b
c d

FIGURE 4.39 (a) A spatial mask and perspective plot of its corresponding frequency domain filter. (b) Filter shown as an image. (c) Result of filtering Fig. 4.38(a) in the frequency domain with the filter in (b). (d) Result of filtering the same image with the spatial filter in (a). The results are identical.

© 1992–2008 R. C. Gonzalez & R. E. Woods

Chapter 4
Filtering in the Frequency Domain

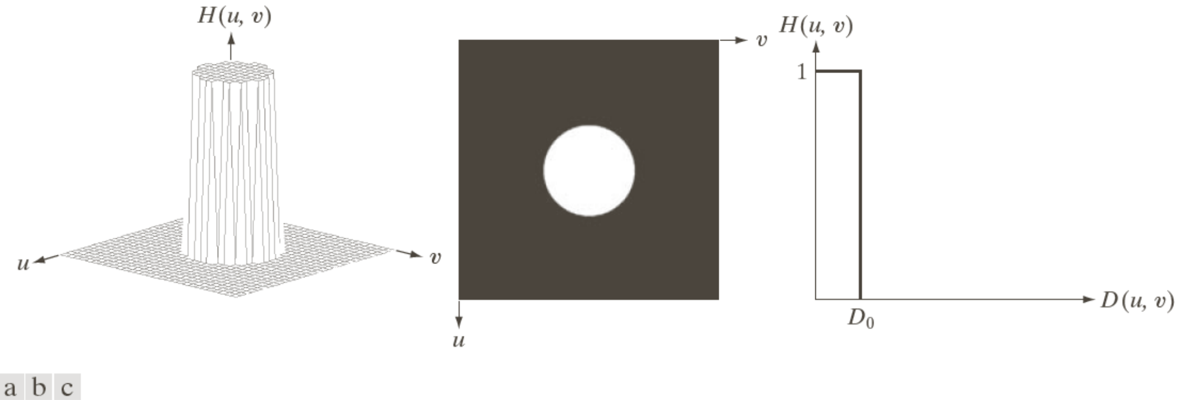

FIGURE 4.40 (a) Perspective plot of an ideal lowpass-filter transfer function. (b) Filter displayed as an image. (c) Filter radial cross section.

© 1992–2008 R. C. Gonzalez & R. E. Woods

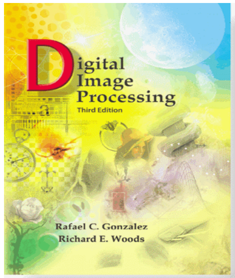

Chapter 4
Filtering in the Frequency Domain

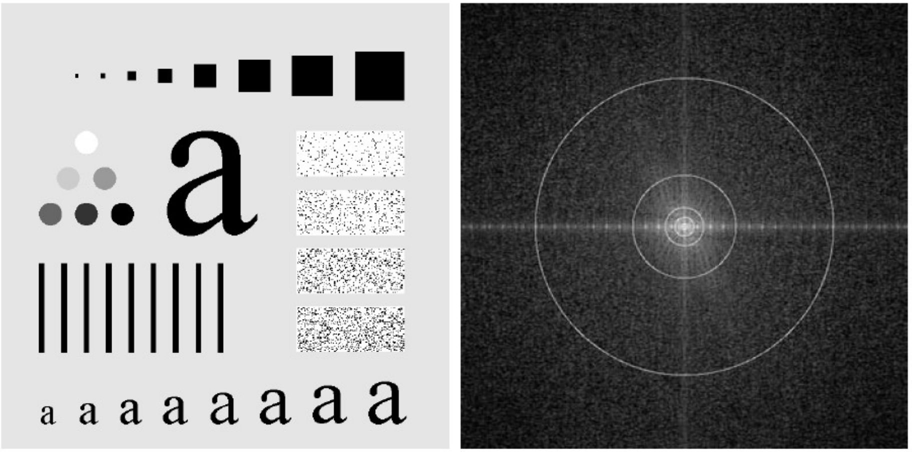

a b

FIGURE 4.41 (a) Test pattern of size 688 × 688 pixels, and (b) its Fourier spectrum. The spectrum is double the image size due to padding but is shown in half size so that it fits in the page. The superimposed circles have radii equal to 10, 30, 60, 160, and 460 with respect to the full-size spectrum image. These radii enclose 87.0, 93.1, 95.7, 97.8, and 99.2% of the padded image power, respectively.

© 1992–2008 R. C. Gonzalez & R. E. Woods

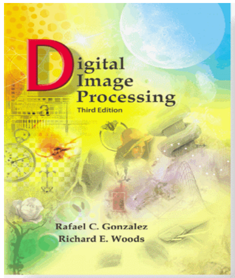

Chapter 4
Filtering in the Frequency Domain

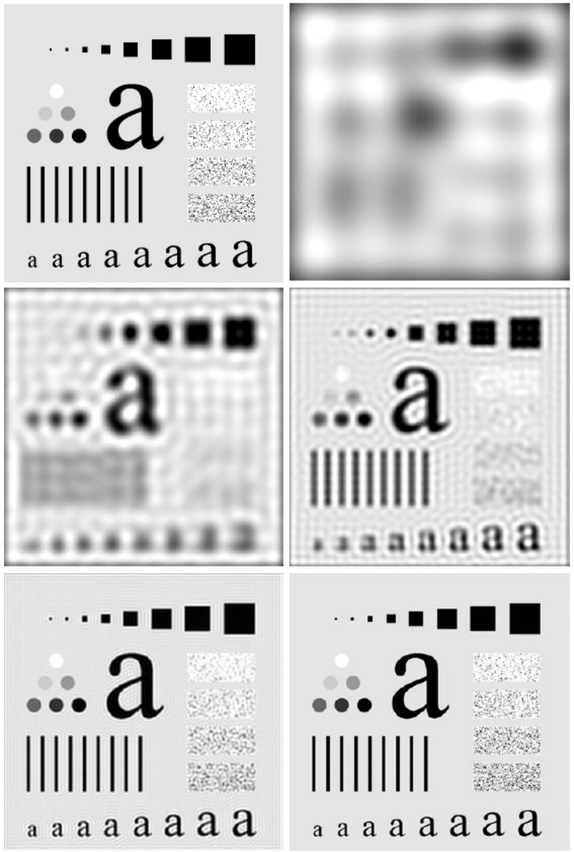

a b
c d
e f

FIGURE 4.42 (a) Original image. (b)–(f) Results of filtering using ILPFs with cutoff frequencies set at radii values 10, 30, 60, 160, and 460, as shown in Fig. 4.41(b). The power removed by these filters was 13, 6.9, 4.3, 2.2, and 0.8% of the total, respectively.

© 1992–2008 R. C. Gonzalez & R. E. Woods

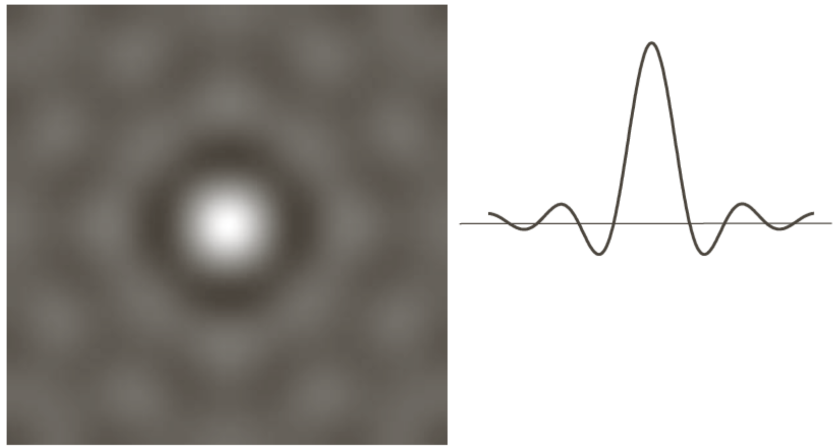

a b

FIGURE 4.43 (a) Representation in the spatial domain of an ILPF of radius 5 and size 1000×1000. (b) Intensity profile of a horizontal line passing through the center of the image.

© 1992–2008 R. C. Gonzalez & R. E. Woods

Chapter 4
Filtering in the Frequency Domain

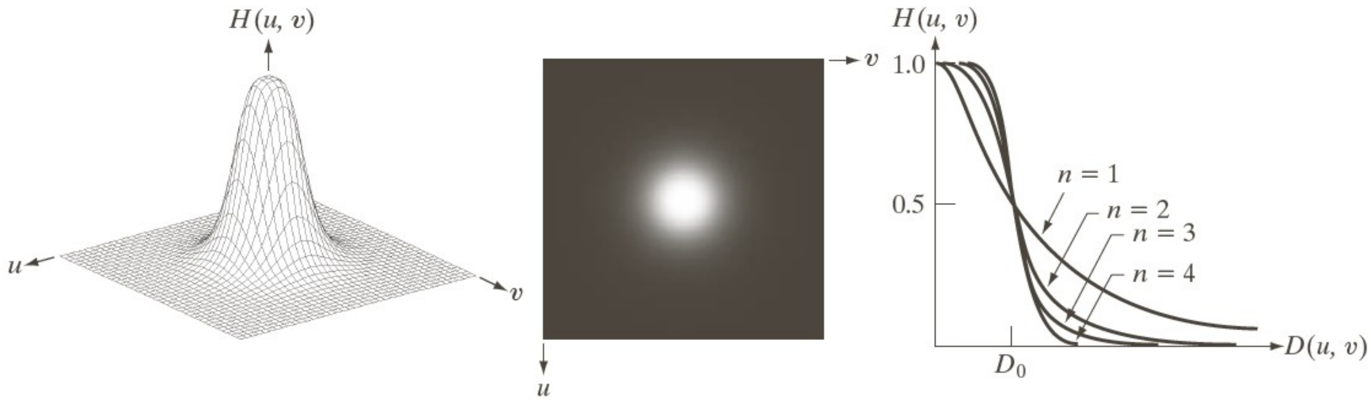

a b c

FIGURE 4.44 (a) Perspective plot of a Butterworth lowpass-filter transfer function. (b) Filter displayed as an image. (c) Filter radial cross sections of orders 1 through 4.

© 1992–2008 R. C. Gonzalez & R. E. Woods

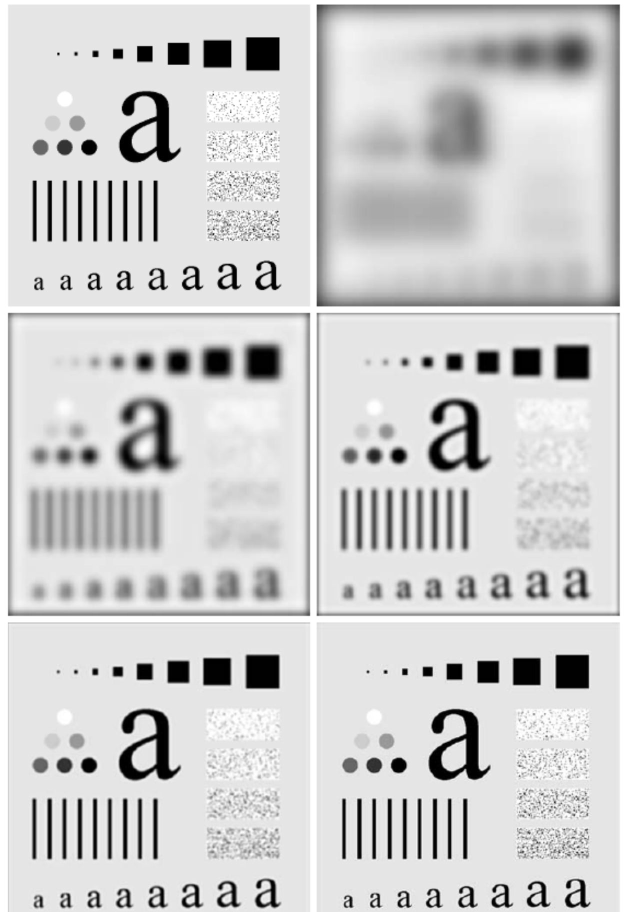

a b
c d
e f

FIGURE 4.45 (a) Original image. (b)–(f) Results of filtering using BLPFs of order 2, with cutoff frequencies at the radii shown in Fig. 4.41. Compare with Fig. 4.42.

© 1992–2008 R. C. Gonzalez & R. E. Woods

Chapter 4
Filtering in the Frequency Domain

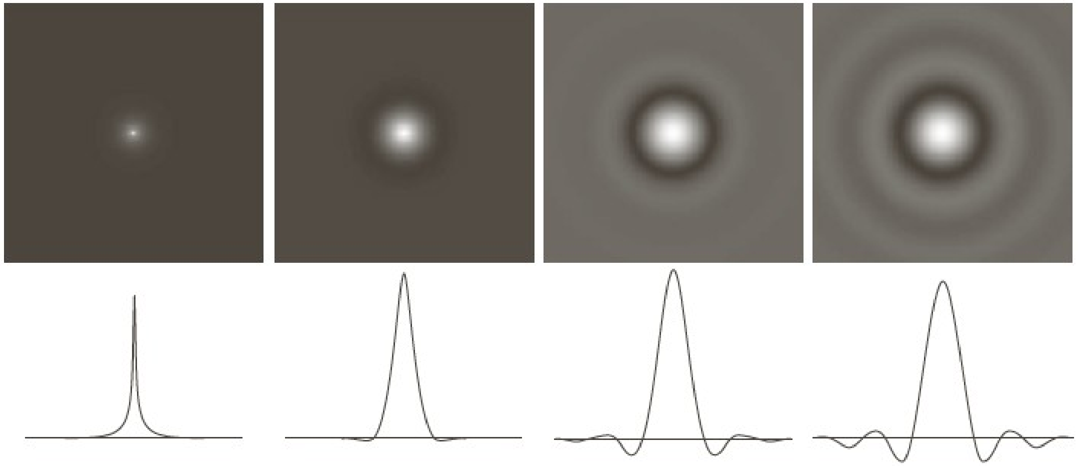

a b c d

FIGURE 4.46 (a)–(d) Spatial representation of BLPFs of order 1, 2, 5, and 20, and corresponding intensity profiles through the center of the filters (the size in all cases is 1000×1000 and the cutoff frequency is 5). Observe how ringing increases as a function of filter order.

© 1992–2008 R. C. Gonzalez & R. E. Woods

Chapter 4
Filtering in the Frequency Domain

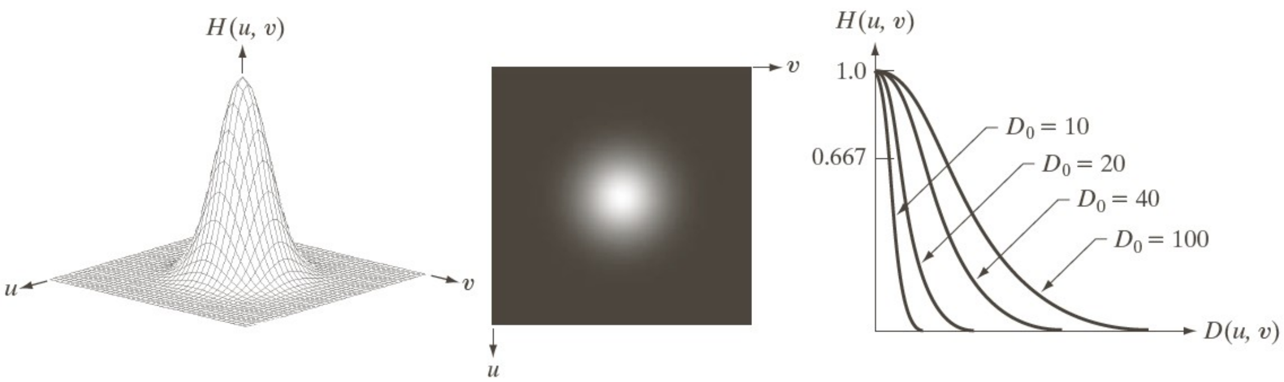

a b c

FIGURE 4.47 (a) Perspective plot of a GLPF transfer function. (b) Filter displayed as an image. (c) Filter radial cross sections for various values of D_0.

© 1992–2008 R. C. Gonzalez & R. E. Woods

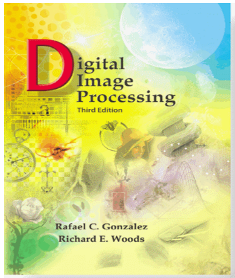

TABLE 4.4
Lowpass filters. D_0 is the cutoff frequency and n is the order of the Butterworth filter.

Ideal	Butterworth	Gaussian
$H(u,v) = \begin{cases} 1 & \text{if } D(u,v) \le D_0 \\ 0 & \text{if } D(u,v) > D_0 \end{cases}$	$H(u,v) = \dfrac{1}{1 + [D(u,v)/D_0]^{2n}}$	$H(u,v) = e^{-D^2(u,v)/2D_0^2}$

© 1992–2008 R. C. Gonzalez & R. E. Woods

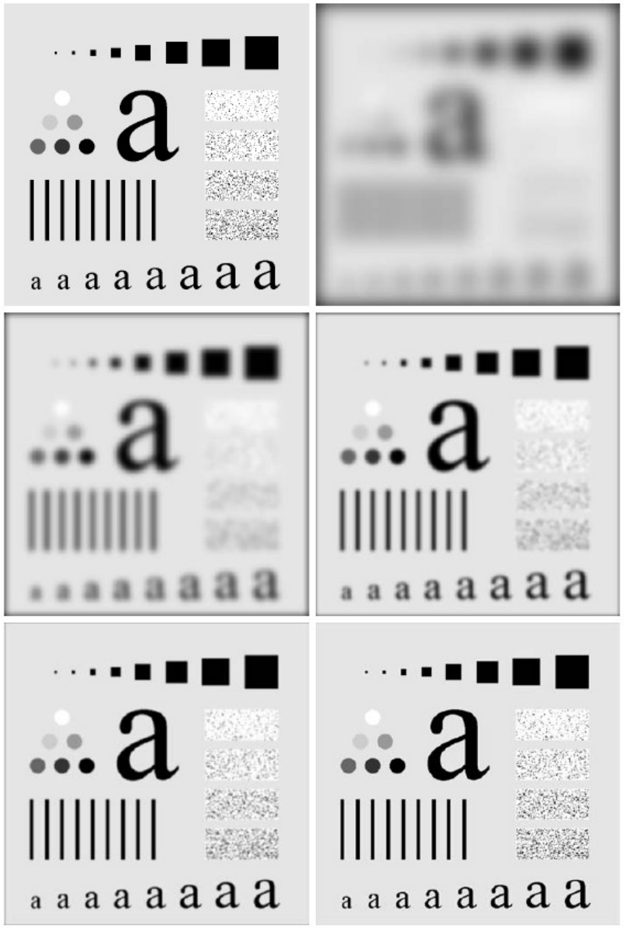

a b
c d
e f

FIGURE 4.48 (a) Original image. (b)–(f) Results of filtering using GLPFs with cutoff frequencies at the radii shown in Fig. 4.41. Compare with Figs. 4.42 and 4.45.

© 1992–2008 R. C. Gonzalez & R. E. Woods

Chapter 4
Filtering in the Frequency Domain

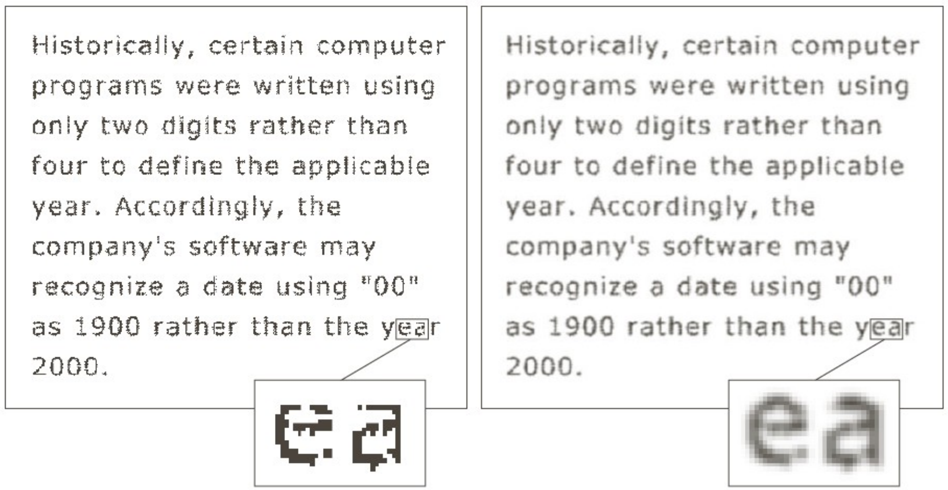

a b

FIGURE 4.49 (a) Sample text of low resolution (note broken characters in magnified view). (b) Result of filtering with a GLPF (broken character segments were joined).

© 1992–2008 R. C. Gonzalez & R. E. Woods

a b c

FIGURE 4.50 (a) Original image (784×732 pixels). (b) Result of filtering using a GLPF with $D_0 = 100$. (c) Result of filtering using a GLPF with $D_0 = 80$. Note the reduction in fine skin lines in the magnified sections in (b) and (c).

© 1992–2008 R. C. Gonzalez & R. E. Woods

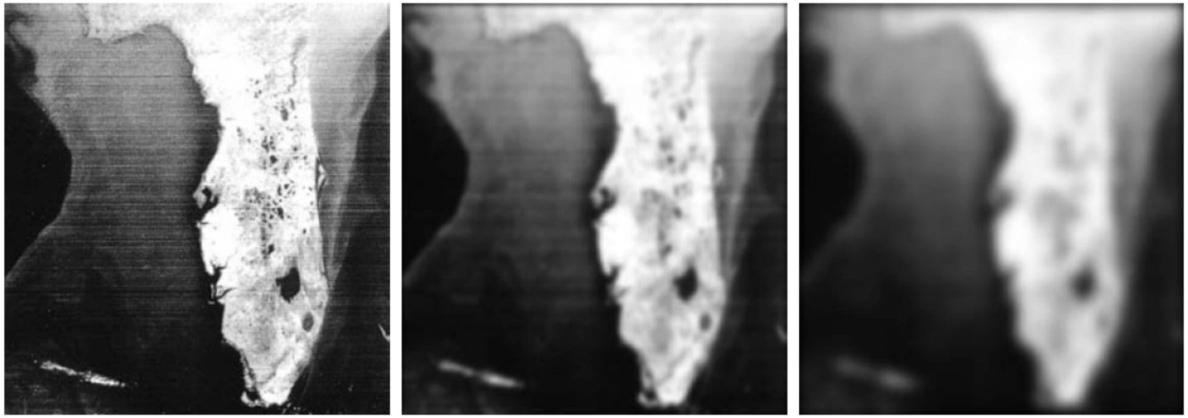

a b c

FIGURE 4.51 (a) Image showing prominent horizontal scan lines. (b) Result of filtering using a GLPF with $D_0 = 50$. (c) Result of using a GLPF with $D_0 = 20$. (Original image courtesy of NOAA.)

© 1992–2008 R. C. Gonzalez & R. E. Woods

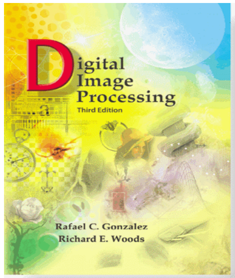

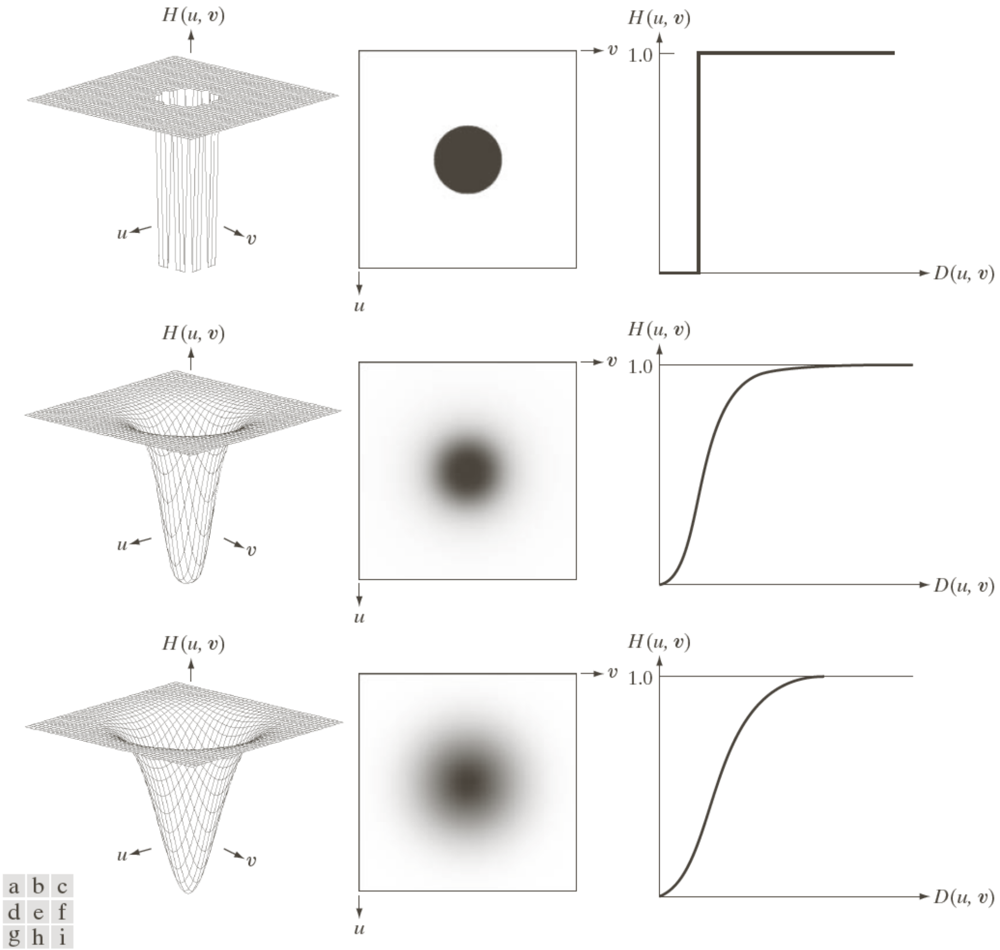

FIGURE 4.52 Top row: Perspective plot, image representation, and cross section of a typical ideal highpass filter. Middle and bottom rows: The same sequence for typical Butterworth and Gaussian highpass filters.

© 1992–2008 R. C. Gonzalez & R. E. Woods

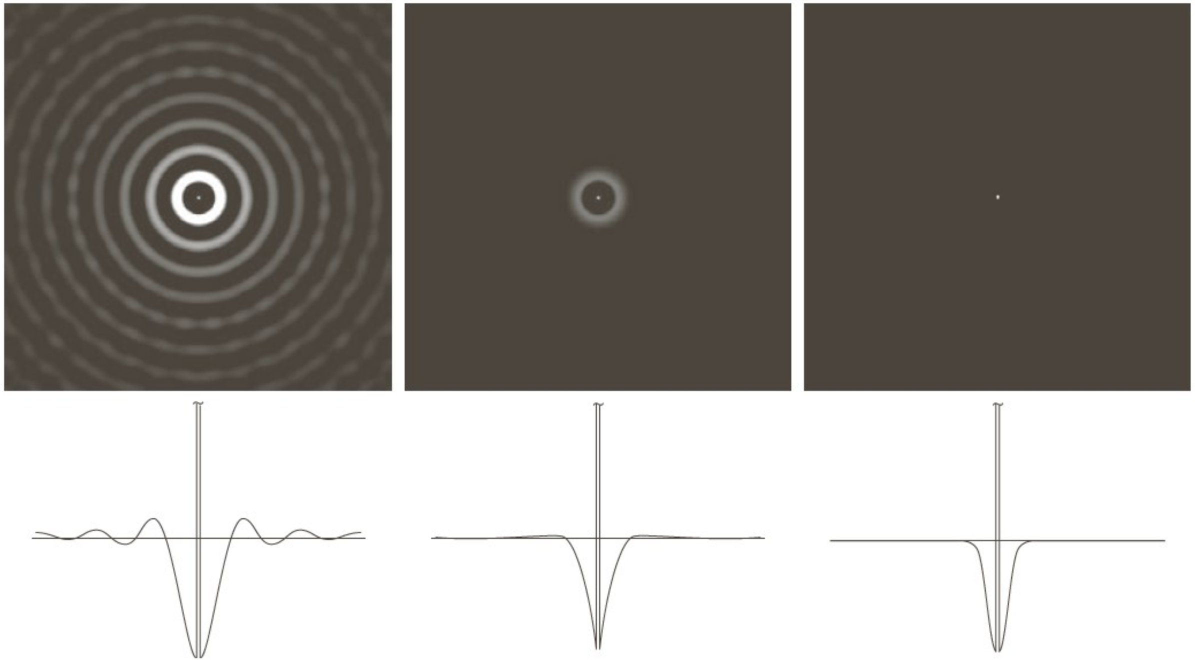

a b c

FIGURE 4.53 Spatial representation of typical (a) ideal, (b) Butterworth, and (c) Gaussian frequency domain highpass filters, and corresponding intensity profiles through their centers.

© 1992–2008 R. C. Gonzalez & R. E. Woods

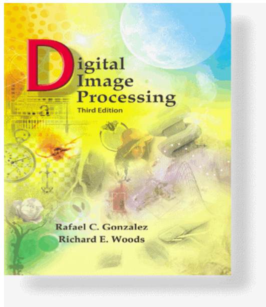

a b c

FIGURE 4.54 Results of highpass filtering the image in Fig. 4.41(a) using an IHPF with $D_0 = 30, 60$, and 160.

© 1992–2008 R. C. Gonzalez & R. E. Woods

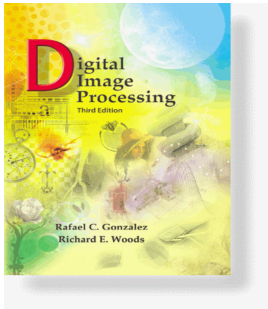

a b c

FIGURE 4.55 Results of highpass filtering the image in Fig. 4.41(a) using a BHPF of order 2 with $D_0 = 30, 60,$ and 160, corresponding to the circles in Fig. 4.41(b). These results are much smoother than those obtained with an IHPF.

© 1992–2008 R. C. Gonzalez & R. E. Woods

a b c

FIGURE 4.56 Results of highpass filtering the image in Fig. 4.41(a) using a GHPF with $D_0 = 30, 60$, and 160, corresponding to the circles in Fig. 4.41(b). Compare with Figs. 4.54 and 4.55.

© 1992–2008 R. C. Gonzalez & R. E. Woods

TABLE 4.5

Highpass filters. D_0 is the cutoff frequency and n is the order of the Butterworth filter.

Ideal	Butterworth	Gaussian
$H(u,v) = \begin{cases} 1 & \text{if } D(u,v) \leq D_0 \\ 0 & \text{if } D(u,v) > D_0 \end{cases}$	$H(u,v) = \dfrac{1}{1 + [D_0/D(u,v)]^{2n}}$	$H(u,v) = 1 - e^{-D^2(u,v)/2D_0^2}$

© 1992–2008 R. C. Gonzalez & R. E. Woods

a b c

FIGURE 4.57 (a) Thumb print. (b) Result of highpass filtering (a). (c) Result of thresholding (b). (Original image courtesy of the U.S. National Institute of Standards and Technology.)

© 1992–2008 R. C. Gonzalez & R. E. Woods

a b

FIGURE 4.58 (a) Original, blurry image. (b) Image enhanced using the Laplacian in the frequency domain. Compare with Fig. 3.38(e).

© 1992–2008 R. C. Gonzalez & R. E. Woods

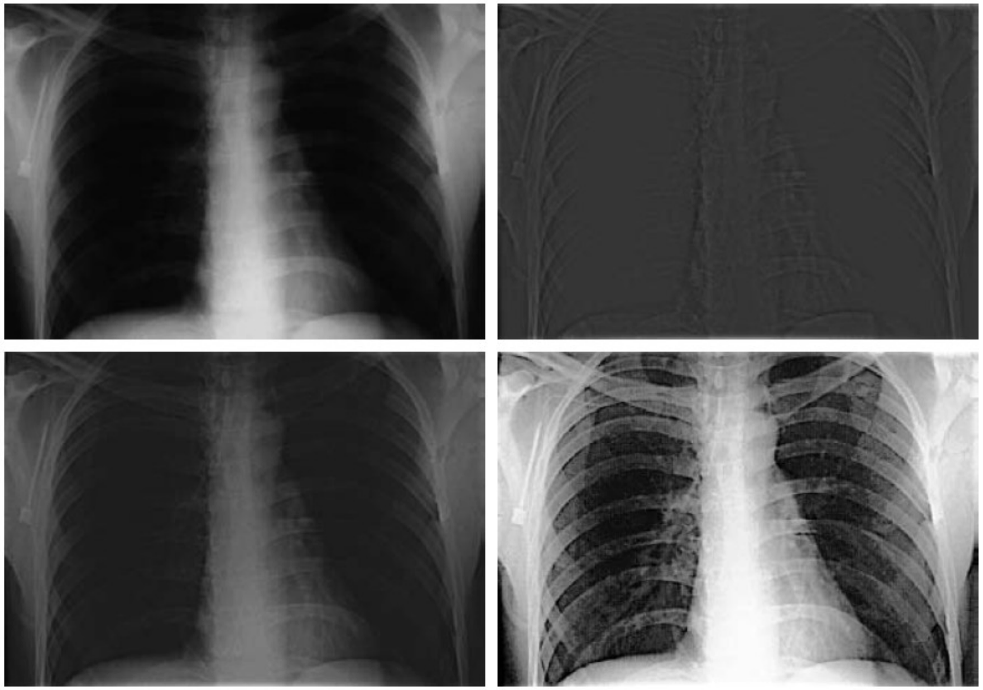

FIGURE 4.59 (a) A chest X-ray image. (b) Result of highpass filtering with a Gaussian filter. (c) Result of high-frequency-emphasis filtering using the same filter. (d) Result of performing histogram equalization on (c). (Original image courtesy of Dr. Thomas R. Gest, Division of Anatomical Sciences, University of Michigan Medical School.)

© 1992–2008 R. C. Gonzalez & R. E. Woods

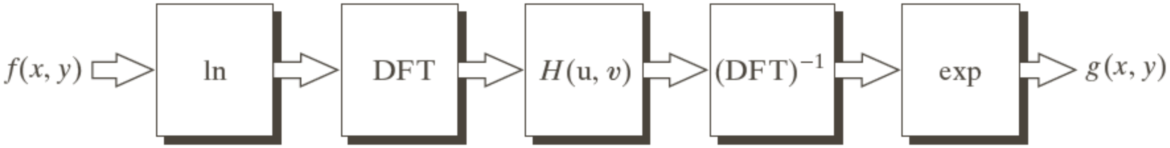

FIGURE 4.60 Summary of steps in homomorphic filtering.

© 1992–2008 R. C. Gonzalez & R. E. Woods

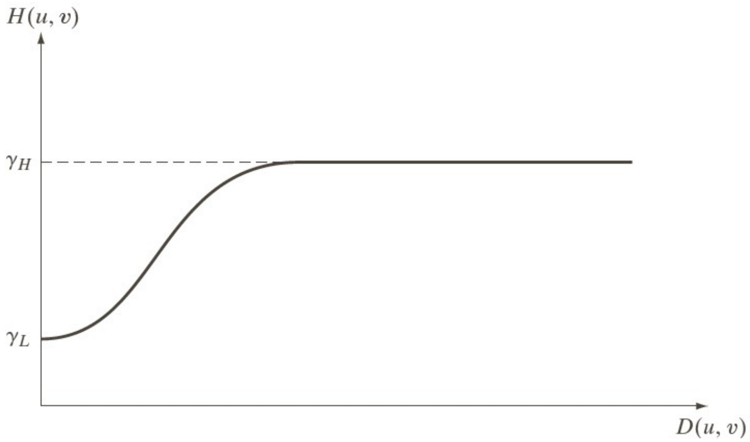

FIGURE 4.61 Radial cross section of a circularly symmetric homomorphic filter function. The vertical axis is at the center of the frequency rectangle and $D(u, v)$ is the distance from the center.

© 1992–2008 R. C. Gonzalez & R. E. Woods

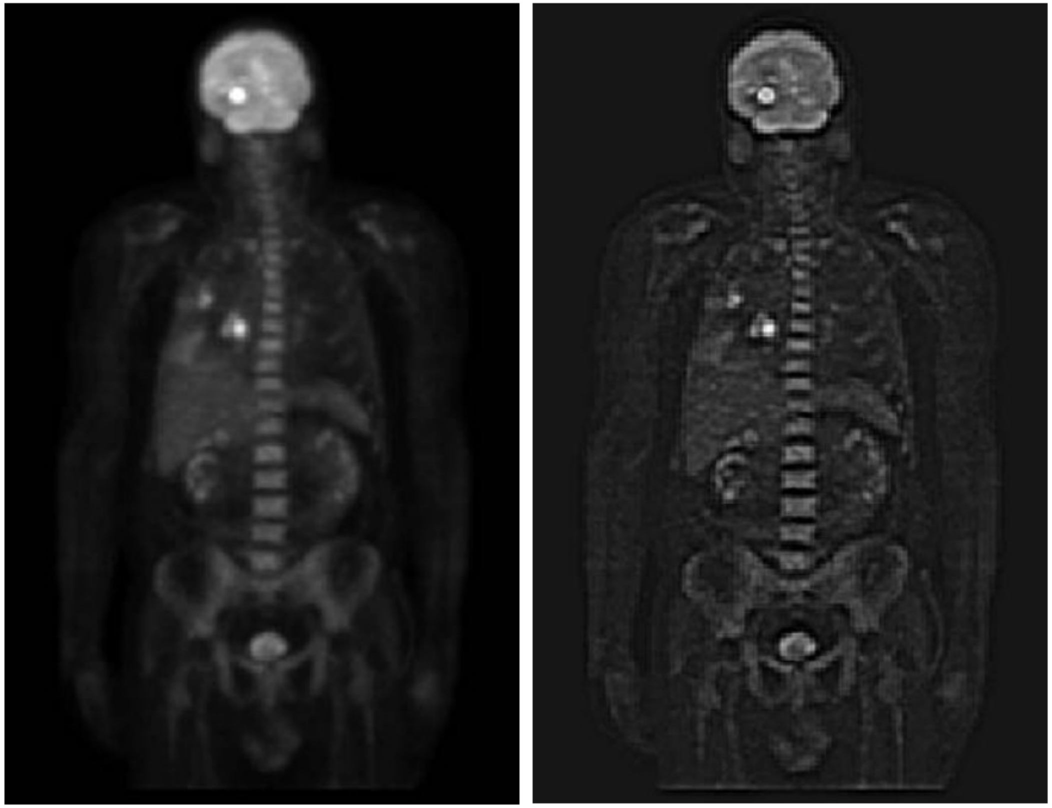

a b

FIGURE 4.62 (a) Full body PET scan. (b) Image enhanced using homomorphic filtering. (Original image courtesy of Dr. Michael E. Casey, CTI PET Systems.)

© 1992–2008 R. C. Gonzalez & R. E. Woods

TABLE 4.6
Bandreject filters. W is the width of the band, D is the distance $D(u, v)$ from the center of the filter, D_0 is the cutoff frequency, and n is the order of the Butterworth filter. We show D instead of $D(u, v)$ to simplify the notation in the table.

Ideal	Butterworth	Gaussian
$H(u,v) = \begin{cases} 0 & \text{if } D_0 - \frac{W}{2} \le D \le D_0 + \frac{W}{2} \\ 1 & \text{otherwise} \end{cases}$	$H(u,v) = \dfrac{1}{1 + \left[\dfrac{DW}{D^2 - D_0^2}\right]^{2n}}$	$H(u,v) = 1 - e^{-\left[\frac{D^2 - D_0^2}{DW}\right]^2}$

© 1992–2008 R. C. Gonzalez & R. E. Woods

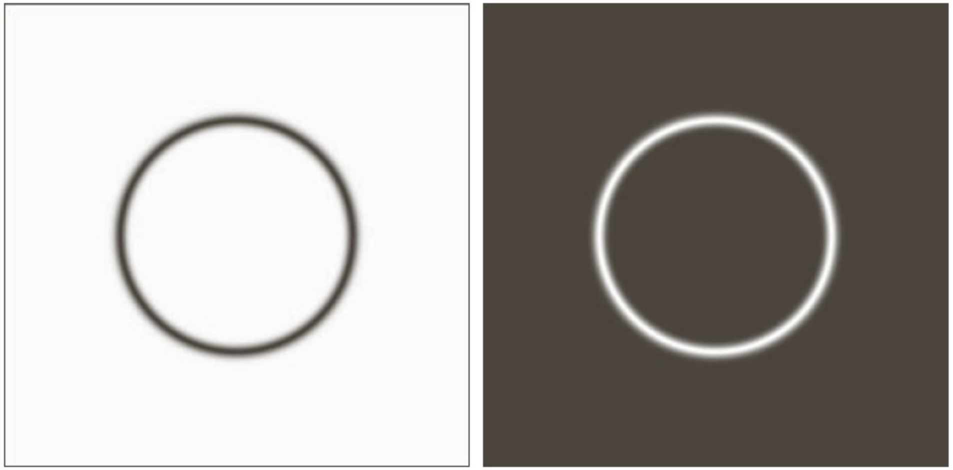

a b

FIGURE 4.63 (a) Bandreject Gaussian filter. (b) Corresponding bandpass filter. The thin black border in (a) was added for clarity; it is not part of the data.

© 1992–2008 R. C. Gonzalez & R. E. Woods

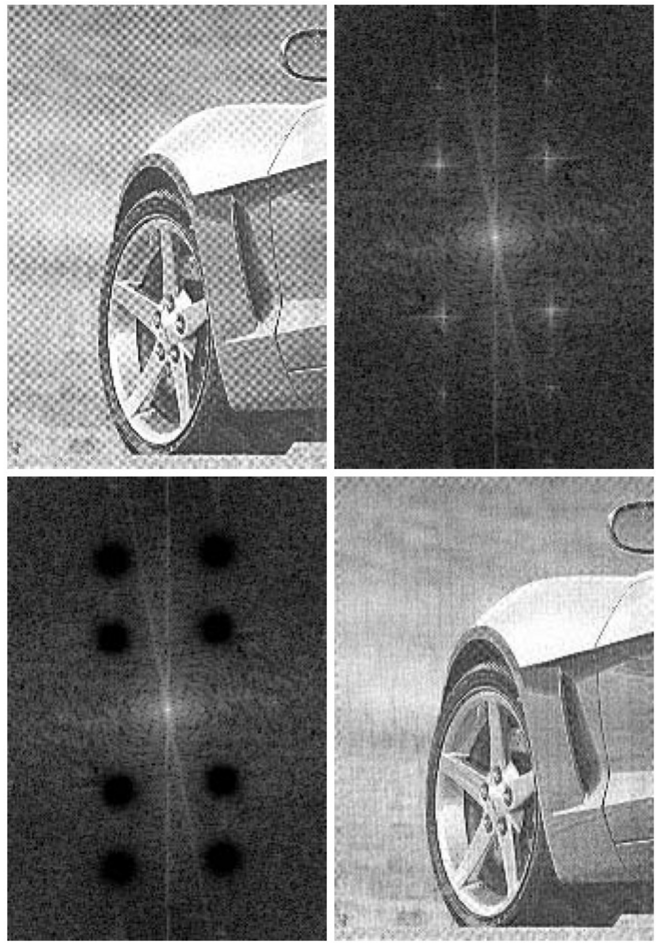

a b
c d

FIGURE 4.64 (a) Sampled newspaper image showing a moiré pattern. (b) Spectrum. (c) Butterworth notch reject filter multiplied by the Fourier transform. (d) Filtered image.

© 1992–2008 R. C. Gonzalez & R. E. Woods

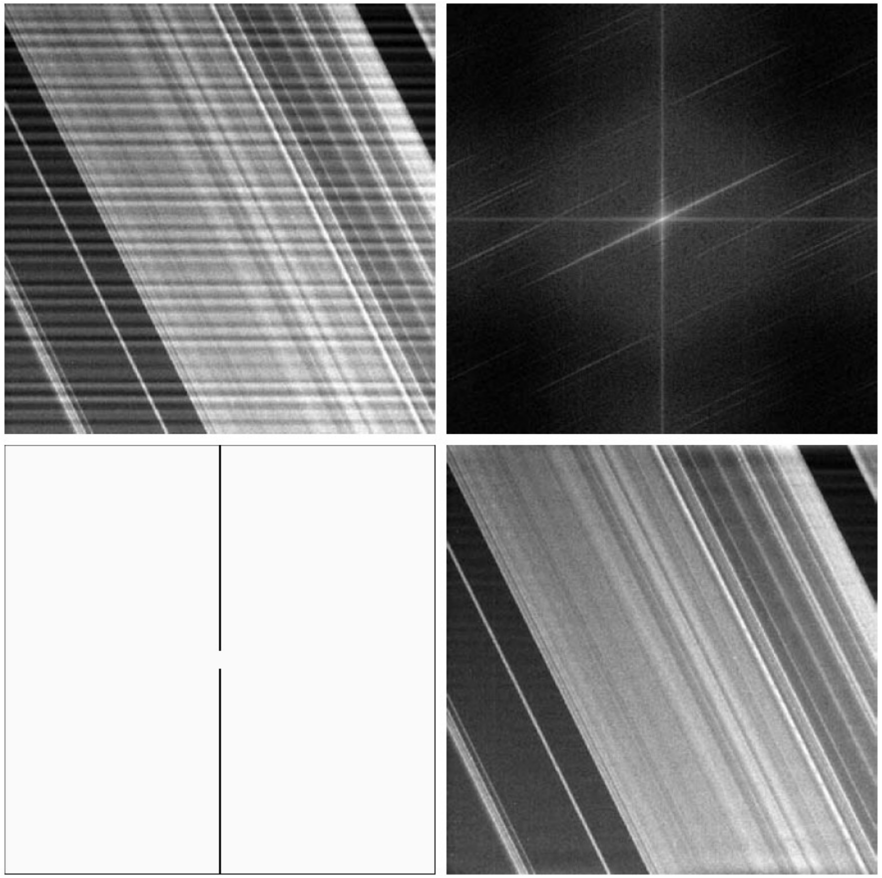

a b
c d

FIGURE 4.65 (a) 674 × 674 image of the Saturn rings showing nearly periodic interference. (b) Spectrum: The bursts of energy in the vertical axis near the origin correspond to the interference pattern. (c) A vertical notch reject filter. (d) Result of filtering. The thin black border in (c) was added for clarity; it is not part of the data. (Original image courtesy of Dr. Robert A. West, NASA/JPL.)

© 1992–2008 R. C. Gonzalez & R. E. Woods

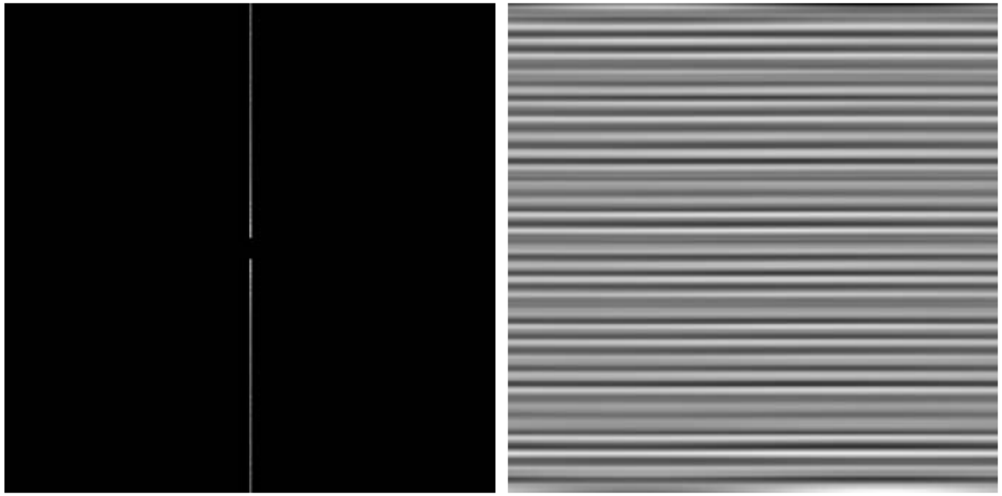

a b

FIGURE 4.66 (a) Result (spectrum) of applying a notch pass filter to the DFT of Fig. 4.65(a). (b) Spatial pattern obtained by computing the IDFT of (a).

© 1992–2008 R. C. Gonzalez & R. E. Woods

Chapter 4

Filtering in the Frequency Domain

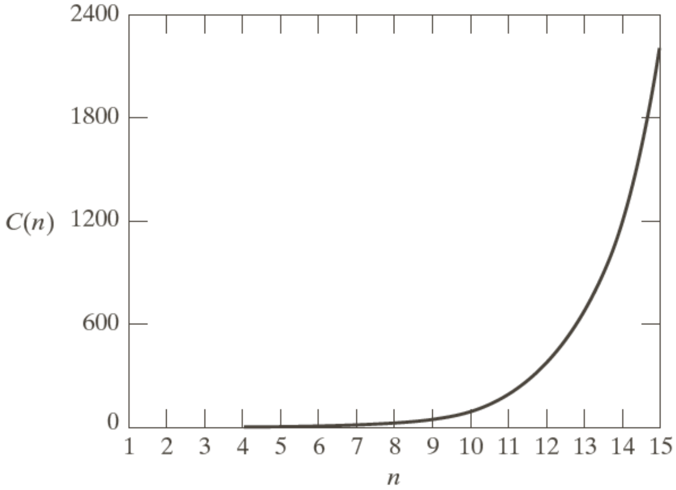

FIGURE 4.67 Computational advantage of the FFT over a direct implementation of the 1-D DFT. Note that the advantage increases rapidly as a function of n.

© 1992–2008 R. C. Gonzalez & R. E. Woods